Conditional Disruption of Hem-1 Results in Impaired Development of Alveolar Macrophages, Pulmonary Alveolar Proteinosis, and Increased Susceptibility to Influenza Virus Infection

Nutthakarn Suwankitwat

A thesis

submitted in partial fulfillment of the

requirements for the degree of

Master of Science

University of Washington

2019

Committee:

Brian M. Iritani

H. Denny Liggitt

Charles Frevert

Jessica Hamerman

Program Authorized to Offer Degree:

Comparative Medicine

University of Washington

Abstract

Conditional Disruption of Hem-1 Results in Impaired Development of Alveolar Macrophages, Pulmonary Alveolar Proteinosis, and Increased Susceptibility to Influenza Virus Infection

Nutthakarn Suwankitwat

Chair of the Supervisory Committee:
Brian M. Iritani
Department of Comparative Medicine

Hematopoietic protein-1 is a hematopoietic cell specific member of the actin-regulatory WAVE (Wiskott-Aldrich syndrome verprolin-homologous protein) complex 2, which acts downstream of many immune receptors and activated Rac to stimulate F-actin nucleation. Mutations in the gene encoding Hem-1 (*NCKAP1L*) have recently been found to result in Primary Immunodeficiency Disease, characterized by recurrent bacterial and viral respiratory infections, skin infections, otitis, and bacteremia. However, the cell-type specific functions of Hem-1 in immune cells are not known. In this study, we generated constitutive and myeloid cell specific *Hem1* knockout mice using the Cre-LoxP system to dissect the importance of Hem-1 in the development and functions of myeloid cells. We found that mice with constitutive or myeloid cell specific disruption of Hem-1 develop pulmonary alveolar proteinosis (PAP), due in part to impaired development of alveolar macrophages (AMs) at the pre-AMs to mature AMs stage. Bronchoalveolar lavage fluid (BALF) from myeloid cell specific *Hem1* null mice contained greatly increased cellular debris, protein, proinflammatory cytokines and chemokines. *Hem1* null neutrophils and monocytes failed to migrate normally in vitro and in vivo to lung tissue in response to LPS or CCL2 stimulation. Myeloid-specific *Hem1* null mice exhibited greatly increased sensitivity to influenza virus infection. These results collectively suggest that Hem-1 is essential for the normal development of alveolar macrophages, and for normal myeloid cell

migration, providing essential new information regarding the mechanisms of how mutations in *NCKAP1L* results in recurring respiratory infections in PID patients.

TABLE OF CONTENTS

LIST OF FIGURES

LIST OF TABLES

LIST OF ABBREVIATIONS

ABCA1- ATP-binding cassette transporter 1

ABCG1- ATP Binding Cassette Subfamily G Member 1

Abi- Abelson interacting protein

AMs- Alveolar Macrophages

ARP2/3- Actin Related Protein 2/3 complex

Bach2- Broad complex-tramtrack-bric a brac and Cap'n'collar homology 2

BALF- Bronchoalveolar lavage fluid

BM- Bone Marrow

BMDMs- Bone Marrow-derived Macrophages

Cre-loxp- Cyclization recombination-locus of X-over P1

CSF2RA- Colony Stimulating Factor 2 Receptor Alpha Subunit

CSF2RB- Colony Stimulating Factor 2 Receptor Beta Common Subunit

GAPDH- Glyceraldehyde 3-Phosphate Dehydrogenase

GM-CSF- Granulocyte Macrophage-colony stimulating factor

Hem1- Hematopoietic protein1

HSPC300- Hematopoietic stem/progenitor cell protein 300

IFNβ- Interferon beta

KC- Keratinocyte chemoattractant (CXCL1)

LPS- Lipopolysaccharide

LTB4- Leukotriene B4

LysM- Lysozyme M

MCP1- Monocyte Chemotactic Peptide-1 (CCL2)

MFI- Mean fluorescence intensity

MIP1a- Macrophage Inflammatory Protein-1 alpha (CCL3)

MIP2- Macrophage Inflammatory Protein-2 (CXCL2)

MOI- Multiplicity of infection

mRNA- Messenger RNA

Nckap1l-Nck associated protein1 like

PBS- Phosphate-buffered Saline

PMNs- Polymorphonuclear cells

PPARg- Peroxisome Proliferator-Activated Receptor Gamma

Sra- Steroid Receptor RNA Activator

TGF-β- Transforming Growth Factor-beta

TGF-βr- Transforming Growth Factor-beta receptor

TLR- Toll-like Receptor

WASP- Wiskott-Aldrich syndrome protein

WAVE- WASp Family Verprolin-homologous Protein

WRC- WAVE Regulatory Complex

ACKNOWLEDGEMENTS

This study was supported by Royal Thai Government Scholarship, National Institute of Animal Health, Department of Livestock Development, and NIH grant RO1AI09020.

I thank Dr. Charles Frevert, Jourdan E Brune, Jessica Felgenhauer, and Timothy Birkland for providing influenza virus and teaching us how to infect mice; Dr. Stephen Libby for his assistance with bacterial experiments; Dr. Denny Liggit for pathology examination; and my thesis committee for their helpful advice and guidance.

Importantly, I thanks to the wonderful research team in Iritani lab: Dr. Terri Iwata, Dr. Alan Avalos, and especially Dr. Heon Park for their advice and assistance with experiments. I would also like to thank my advisor Dr. Brian Iritani, without whom this research could not been completed.

Finally, I must express my very profound gratitude to my parents, my teachers, my partner, and my friends for providing me with unfailing support and continuous encouragement during the years of researching and writing this thesis. This accomplishment would not have been possible without them. Thank you.

DEDICATION

This study is dedicated to all mice in the research.

INTRODUCTION

Actin cytoskeleton reorganization is essential for many "active" aspects of immune responses to infection, including formation of the immunological synapse, adhesion of immune cells to the vascular endothelium, emigration to infection sites, and formation of phagosomes and phagocytosis of foreign agents. At the heart of these processes is the active, coordinated, directional polymerization and depolymerization of filamentous actin (F-actin), which is initiated by many important immune receptors including B and T cell antigen receptors, chemokine, toll-like receptors, cytokine receptors, and integrins (1). Receptor-ligand interaction leads to activation of Guanine nucleotide exchange factors (GEFs) such as Vav, Dock2, and Dock8, which then activate Rho family of GTPases (including Rac (Rac1-3), Cdc42, and RhoA) by converting inactive Rho-GDP to the active Rho-GTP form (2). Genetic studies in *Drosophila* and *C. elegans*, suggest that the WASp (Wiskott-Aldrich Syndrome protein) adaptor protein is a key downstream target of CDC42. In contrast, the Rac GTPases predominantly activate the WAVE (WASP Family verprolin homologous protein) adaptor complex-1 or-2 (3). In mammalian cells, the WAVE complex consists of multiple subunits including WAVE (-1, -2, or -3); HSPC300, Abi (-1 or -2); Hem (-1 [Nckap1-like] or -2 [Nckap1]); and Sra1 (CYFIP1). In hematopoietic cells only the WAVE2 complex (consisting of WAVE2, HSPC300, SRA-1, and Hem-1) is present. Of the WAVE2 complex members, only *Hem1* is exclusively expressed in hematopoietic cells. In response to active GTP-bound Rac, the WAVE complex activates the Arp2/3 complex, which stimulates actin nucleation and induction of actin-regulated processes.

The importance of regulated actin polymerization and depolymerization in protective immunity is underscored by the observations that mutations in actin-regulatory proteins can result in Primary Immunodeficiency Disease (PID), whereby components of the immune system

are either missing or are dysfunctional resulting in severe immunodeficiency disease that often progresses to autoimmune disease or cancer (4). For example, loss-of-function mutations in the *WASp* gene result in Wiskott-Aldrich Syndrome, a rare inherited X-linked recessive disease characterized by opportunistic viral and bacterial infections, microthrombocytopenia, atopic dermatitis, and increased susceptibility to autoimmune disease and cancers (including B cell lymphoma and leukemias) (5). WASp mutations result in a number of immunological defects including decreased number and functions of T cells, alterations in the representation of specific Ig isotypes, defective antibody responses to vaccines, decreased regulatory T cell functions, and impaired myeloid cell migration (see (6) for review). Loss of function mutations in other genes encoding proteins involved in actin assembly or disassembly including WIP (WASp interacting protein), Rac2, Dock2, Dock8 also have been noted to cause PIDs with similar clinical manifestations. Although mutations in WAVE complex proteins resulting in PID had not been previously recognized, 4 human kindreds were recently identified whereby loss of function variants in *NCKAPL1* encoding Hem-1 resulted in PID. Affected children presented with severe immunodeficiency resulting in recurrent bacterial and viral skin infections, septic arthritis, bacteremia, otitis media, and respiratory infections leading to bronchiectasis. Initial analyses of 5 individuals revealed impaired T cell activation, altered cytokine expression, reduced migration of T cells and neutrophils, and poor specific antibody responses ((7)). These results suggest that Hem-1 likely has key roles in the development and/or functions of many immune cell types. Interestingly, GWAS studies indicated that alterations in expression of *NCKAP1L* are linked to inflammatory bowel disease (IBD) in humans (8), and high expression of *NCKAP1L* is associated with poor prognosis in chronic lymphocytic leukemia (9). Thus, understanding the

normal functions of Hem-1 in specific immune cell types has implications in PID, IBD, and cancer.

Biochemical and genetic analyses in *D. melanogaster, C. elegans, Arabidopsis*, and *Dictyostelium* suggest that homologs of Hem-1 act downstream of Rac to regulate actin polymerization, migration, and cell shape changes that are important for normal morphogenesis and development (10)(11)(12)(13). Similarly, knockdown of Hem-1 in a neutrophil like cell line results in impaired actin polymerization and decreased motility due to failure to propagate waves of actin polymerization at the leading edge of the cells (14). Mice with a chemically-induced non-coding point mutation in *Hem1* exhibit a plethora of immunological defects due to defective actin polymerization, including neutrophilia, lymphopenia, impaired T cell development and activation, reduced B cell numbers, reduced chemotactic response of neutrophils, and increased production of proinflammatory cytokines, consistent with the phenotypes seen in PID patients (15). Studies in neutrophil-like cell lines, mice, and humans with non-coding mutations in *Hem1* indicate that loss of Hem-1 protein results in destabilization of the WAVE complex, and subsequent proteolysis of the remaining complex members.

Because of the widespread immune dysregulation in both human and mice with PID due to mutations in *Hem1*, we sought to develop a system to specific disrupt Hem-1 in specific immune cells to uncover the cell-type specific requirements for Hem-1 and the WAVE complex in overall immunity. Utilizing the Cre-LoxP system, we generated both constitutive and myeloid cell specific *Hem1* deficient mice. Our results reveal that Hem-1 is required for the normal development and function of AMs, the most abundant innate immune cell in the alveolar space. AMs are first line defenders against respiratory pathogens and are essential for normal clearance of surfactant. Disruption of Hem-1 results in a buildup of cell debris and protein (Pulmonary

Alveolar Proteinosis (PAP)), and greatly increased sensitivity to influenza virus infection. These results provide the first description of the importance of Hem-1 in the development and function of AMs and provide a cellular mechanism for why mutations in Hem-1 result in increased sensitivity to respiratory pathogens.

.

RESULTS

Generation of constitutive and myeloid cell specific conditional Hem1 null mice

In order to delete *Hem1* in a cell-type specific manner, we obtained a C57BL6J *Nckap1l floxed*-targeting construct from the Knockout Mouse Project (KOMP), whereby exons 12-16 of *Nckap1l* are flanked by *loxP* sites (Figure 1A). The *Nckap1l* targeting vector was electroporated into G4 ES cells (129S6/SvEvTac x C57BL/6Ncr F1 hybrid cells). 6 clones were tested by southern blot and were confirmed to be correctly targeted to the *Nckap1l* locus (Figure 1B). 3 clones were injected into C57BL6/J embryos generating 3 founder lines of *Nckap1l "*pre-conditional" chimeric (*Nckap1*$^{tm1a(KOMP)/Wtsi}$) mice. "Conditional" *Nckap1l (herein Hem1)*$^{fl/+}$ mice, were generated by crossing *Hem1* pre-conditional mice with *FLPER* recombinase mice which recognized *FRT* sites resulting in the deletion of the *β-gal* and *neo* cassettes. To generate "constitutive" *Hem1*$^{-/-}$ mice, pre-conditional mice were bred *Mox2*-Cre, which deleted exons 12-16 and *Neo* cassette in germline cells. *Hem1* deletion was confirmed by PCR and immunoblotting.

In order to dissect the importance and functions of Hem-1 in myeloid cells, we bred *Hem1 floxed* mice to *Lyz2*-Cre (also known as *LysM*Cre) mice, which express the Cre enzyme in myeloid cells (macrophages, monocytes, neutrophils), and to a lesser extend in dendritic cells (16). We generated mice that were heterozygous (*Hem1*$^{fl/fl}$ *LysMcre*$^{+}$) or homozygous for *LysMcre* (*Hem1*$^{fl/fl}$ *LysMcre*$^{+/+}$) and thus express higher levels of the Cre enzyme. Analyses of purified BM derived macrophages (BMDM) using semi-quantitative PCR indicates that we are able to achieve ~70% deletion in *Hem1*$^{fl/fl}$ *LysMcre*$^{+}$ mice and ~85% deletion in *Hem1*$^{fl/fl}$ *LysMcre*$^{++}$ mice (Figure 1C). To more specifically test for Cre expression in different populations of myeloid cells, *Hem1floxed* mice to tdTomato mice (Rosa26$^{\text{lox-stop-lox-}tdTomato}$),

whereby red fluorescent protein (RFP) is expressed upon Cre-mediated deletion of a stop-codon, thus allowing Cre-expressing cells to be identified and tracked using flow cytometry(17). Analysis of *Hem1*$^{fl/fl}$*LysMcre*$^{+}$ mice indicates strong Cre-mediated deletion in immature and mature neutrophils (>95%), as well as large and small peritoneal macrophages (LPM and SPM), and alveolar macrophages (AMs) (Figure 1D). *LysMcre*$^{+}$ activity in monocytes and immature neutrophils appear less strong but still significant ~60-75%. These results show that *Hem1* is conditionally disrupted in myeloid cells from *Hem1*$^{fl/fl}$*LysMcre*$^{+}$ mice.

Whole body deletion of Hem1 results in neutrophilia, lymphopenia, and a reduction in alveolar macrophages.

We first examined the immunological phenotypes of mice with constitutive "tissue-wide" deletion of *Hem1* since this model may more accurately reflect the phenotypes of humans with non-coding mutations in *Hem1*. *Hem1*$^{-/-}$ mice presented with neutrophilia, eosinophilia, and lymphopenia (Figure 2A), which paralleled the phenotypes of mice containing a non-coding point mutation in *Hem1* (*Hem1*$^{pt/pt}$ mice)(18). This was associated with increased total white blood cells (WBCs) in the BM (Figure 2B) and reduced WBC numbers in the spleen at ~8 weeks of age (Figure 2C). As *Hem1*$^{-/-}$ mice age, splenocyte cell number increased due to extramedullary hematopoiesis, likely resulting from increased release of hematopoietic stem cell and progenitors from the bone marrow niche(18)(19). Further analyses revealed increased numbers of pre-neutrophils, immature neutrophils, and mature neutrophils in BM, spleen, and blood (Figure 2E). The number of BM monocytes and LPMs were also increased in the BM and peritoneum respectively (Figure 2F). Interestingly, despite the increase in BM monocytes, the number of alveolar macrophages in bronchoalveolar lavage fluid (BALF) were significantly

decreased, which correlated with increased debris and opaque "milky" appearance of BAL fluid (Figure 2F). As with *Hem1*$^{pt/pt}$ mice, *Hem1*$^{-/-}$ mice were more sensitive to opportunistic infections with bacteria such as *Pasteurella pneumotropica*. Gross and histological examination of *Hem1*$^{-/-}$ mice revealed a spectrum of lesions, including dense amyloid accumulations containing foci of mineral at the margins of the liver, extramedullary hematopoiesis with lymphoid depletion, myeloid hyperplasia in bone marrow; multifocal mineralization in heart, lungs, epididymis; periodontitis with adherent bacteria, and dermatitis with multifocal mineralization (Figure 3). These results collectively indicate that constitutive loss of *Hem1* recapitulated the phenotypes associated with *Hem1* point mutation mice and are consistent with the phenotypes of children with PID due to mutations in *Hem1*.

Conditional disruption of Hem1 in myeloid cells results in increased numbers of developing monocytes and neutrophils in the bone marrow but decreased number of alveolar macrophages.

To determine the cell autonomous functions of Hem-1 in the development and homeostasis of myeloid cells, we assessed the numbers of developing and mature myeloid cells in peripheral blood, bone marrow, spleen, and BALF from *Hem1*$^{fl/fl}$*LysMcre*$^{+}$ and *Hem1*$^{fl/fl}$*LysMcre*$^{++}$ mice relative to *Hem1*$^{fl/fl}$*LysMcre*$^{-}$ and *Hem1*$^{+/+}$*LysMcre*$^{+}$ or $^{+/+}$ control mice. Surprisingly, we found a decrease in lymphocyte number in peripheral blood (PB) from *Hem1*$^{fl/fl}$*LysMcre*$^{+}$ mice relative to *Hem1*$^{fl/fl}$ control mice (Figure 4A). In contrast, the total number of WBCs, pre-neutrophils, immature neutrophils, and monocytes were increased in the BM (but not spleen and PB) compared to the control mice (Figures 4B, D, E, F, and G). Similar to *Hem1*$^{-/-}$ mice, the number of WBCs and tissue resident alveolar macrophages in BALF were significantly decreased (~5

fold) in *Hem1*$^{fl/fl}$*LysMcre*$^{+}$ mice relative to *Hem1*$^{+/+}$*LysMcre*$^{+}$ control mice (Figure 4C, H). This also correlated with an increase in CD45.2^{neg} cell debris in BALF, resulting in increased optical density and an opaque appearance to the fluid (Figure 4I, J, K). Importantly, total protein and lipid in BALF were increased in *Hem1*$^{fl/fl}$*LysMcre*$^{+}$ mice relative to the control (Figure 4L, J bottom), indicating pulmonary alveolar proteinosis (PAP) condition. Interestingly, EpCAM (CD326) were increased in BALF from *Hem1*$^{fl/fl}$*LysMcre*$^{+}$ mice relative to the control (Figure 4M), consistent with increased sloughed epithelial cells in BALF . Analyses of the remaining AMs indicated that they are larger in size based on increased forward light scatter (FSC) characteristics (Figure 4N). These results collectively suggest Hem-1 is important for the development and/or homeostasis of neutrophils, monocytes, and alveolar macrophages.

Hem1 is required for the development of alveolar macrophages

Given that both constitutive and myeloid cell-specific deletion of *Hem1* resulted in a reduction of mature AMs, we next addressed whether *Hem1* might be important for AM development. AMs develop during embryogenesis beginning around embryonic day 15 when fetal monocytes/macrophages migrate from fetal liver to lungs presumably via the bloodstream, at which point the cells further differentiate to pre-AMs, characterized by downregulation of Ly6C and upregulation of CD11c (Figure 5A). In response to GM-CSF produced by alveolar epithelial cells, pre-AMs upregulate the nuclear receptor *Pparγ*, which induces a transcriptional program that instructs the development and function of pre-AMs to mature AMs. To define further where AM development is effected following disruption of *Hem1*, we harvested lung and liver cells from post-natal day 3 (PND3) WT and *Hem1*$^{-/-}$ pups, when AM development was previously shown to be maximal (20). Utilizing specific flow cytometric markers (SiglecF, CD11c, CD11b,

F4/80, Ly6c) to distinguish different stages of AM development, we found equivalent frequencies of fetal monocytes, and pre-alveolar macrophages (pre-AMs) in the lungs from WT and *Hem1*$^{-/-}$ mice (Figure 5C). However, the percent of AMs were decreased significantly in *Hem1*$^{-/-}$ versus WT lung tissues (Figure 5C), while the percentages of monocytes and macrophages were increased in *Hem1*$^{-/-}$ compared to WT livers (Figure 5D). In addition, analyses of BALF from mature 8 wk old *Hem1*$^{fl/fl}$*LysMcre*$^{+}$ and *LysMcre*$^{+}$ mice revealed that the ratio of mature AMs to pre-AMs was reduced by 90%, consistent with impaired maturation (Figure 5E).

To determine why AM development might be effected, we assessed levels of AM differentiation factors including GM-CSF, TGFβ, Bach2, and *PPARg* in purified AMs from WT and *Hem1*$^{fl/fl}$ *LysMcre*$^{+/+}$ mice. We found that GM-CSF and Bach2 mRNA levels were increased in *Hem1*$^{-/-}$ relative to WT AMs. However, *PPARg* levels were decreased following disruption of *Hem1* (Figure 5F). To determine whether cytokine receptors are affected, we also measured levels of CSF2RA, CSF2RB, TGFβr1, and TGFβr2 in AMs. We found that the receptors were normal or increased in *Hem1*$^{fl/fl}$ *LysMcre*$^{+/+}$ mice (Figure 5F). These results suggest that disruption of *Hem1* results in a defect on the development of AMs from the pre-AMs to AMs stage, likely due to impaired abilities to upregulate *PPARg* and/or defective migration of pre-AMs to expose to the GM-CSF at the appropriate location in alveoli.

Neutrophils from myeloid-specific Hem1 deficient mice fail to polymerize F-actin efficiently. Because Hem-1 and the WRC have been implicated in reorganization of the actin cytoskeleton, we next determined whether conditional disruption of *Hem1* in AMs and neutrophils impacts F-actin polymerization. BM neutrophils isolated from *Hem1*$^{fl/fl}$ *LysMcre*$^{+}$ and WT mice were stimulated with fMLP, (a potent chemotactic factor for neutrophils) followed by intracellular

(IC) flow cytometric staining with fluorescent-conjugated phalloidin. In comparison to WT neutrophils, *Hem1*$^{fl/fl}$ *LysMcre*$^{+}$ neutrophils fail to increase phalloidin intensity relative to unstimulated cells (Figure 6A). Analysis of neutrophils from *Hem1*$^{fl/fl}$ *LysMcre*$^{+}$ *tdTomato*+ mice stained with fluorescence-conjugated phalloidin and imaged by fluorescent microscope revealed that tomato positive (Cre expressing) cells exhibited decreased actin-polarization at cell-cell contact sites relative to tomato negative cells, where fluorescent intensity was decreased and was distributed more diffusely around the cell membrane (Figure 6B). These results suggest that *Hem1* is required for F-actin polymerization and actin polarization in neutrophils.

Macrophages and neutrophils from myeloid cell specific Hem1 deficient mice phagocytose bacteria and particles normally in vitro but exhibit reduced phagocytosis in vivo.

Because reorganization of the actin cytoskeleton has been implicated as being important for phagocytosis by macrophages and neutrophils in part by inducing formation of the phagocytic cup, we investigated if loss of *Hem1* in myeloid cells results in impaired phagocytosis both *in vitro* and *in vivo*. We first assessed the abilities of bone marrow derived macrophages (BMDMs) to phagocytose 1μm fluorescent-conjugated beads. Surprisingly, we found that *Hem1*$^{fl/fl}$*LysMcre*$^{+}$ BMDMs were able to phagocytosis the particles equally well compared to *LysMcre*$^{+}$ control mice 60 minutes post-feeding (Figure 6C). *Hem1*$^{fl/fl}$*LysMcre*$^{+}$ macrophages were also able to phagocytose labeled Zymosan, a ~3 μm yeast cell wall component that requires internalization for the fluorescence to be emitted, equally well as control macrophages at 37^{o}C, although zymosan uptake was reduced at 4^{o}C in *Hem1*$^{fl/fl}$*LysMcre*$^{+}$ BMDM relative to control macrophages (not shown).

To examine the abilities of Hem-1 deficient macrophages to phagocytose *in vivo*, mice were stimulated with LPS to recruit inflammatory cells followed by fluorescent beads instillation via oropharyngeal (o.p.) route under anesthesia. BAL fluids were then collected 30 minutes post-bead administration and were stained with anti-CD64 antibodies for flow cytometric analyses. We found that *Hem1*-deficient alveolar macrophages had reduced uptake of fluorescent beads (Figures 6D) in vivo, possibly due to non-cell autonomous effects on uptake, or an effect on AMs migration. Peritoneal macrophages from *Hem1*$^{fl/fl}$*LysMcre*$^{+}$ mice similarly exhibited impaired abilities to phagocytose beads *in vivo* compared to WT controls 30 minutes post-intraperitoneal (i.p.) administration (Figure 6E). Neutrophils consistently also had a defect in phagocytosis after inducing neutrophils recruitment into lavage fluids with LPS instillation via oropharyngeal administration (Figure 6F). These results suggest that disruption of Hem-1 does not directly inhibit the abilities of macrophages and neutrophils to phagocytose bacteria and beads in the size range of 1-3 μm, but that in vivo engulfment of bacteria and particles are reduced, likely due to impaired migration and/or increased cell death.

Hem-1 deficient neutrophils and monocytes fail to migrate efficiently in response to chemokines

We next investigated whether loss of Hem-1 affects the abilities of neutrophils to migrate in response to chemokine stimulation, using time-lapse video microscopy. Purified neutrophils from *Hem1*$^{fl/fl}$*LysMcre*$^{+}$ and littermate control mice were loaded into μ-slide chemotaxis chambers, and cell migration in response to the LTB4 chemoattractant and PBS control were assessed and recorded for 2 hours (Figure 7A). The cell viability after purification was not different between two groups (not shown). The loss of Hem-1 resulted in significantly reduced

velocity and distance traveled, whereas forward migration index and directness were not affected (Figure 7B-E). To assess the abilities of neutrophils to migrate *in vivo*, we administered LPS via oropharyngeal delivery under anesthesia and assessed neutrophil numbers in BALF and peripheral blood before and 2 hours after stimulation. We found increased numbers of neutrophils in peripheral blood and reduced numbers in BAL fluid from *Hem1*$^{fl/fl}$*LysMcre*$^{+}$ mice compared to WT mice (Figure 7F, G), consistent with increased neutrophil production and impaired migration. To determine whether the reduced *in vivo* neutrophil migration following Hem-1 disruption is cell autonomous, we purified Tomato^{+} neutrophils from CD45.2^{+} *Hem1*$^{fl/fl}$*LysMcre*$^{+}$*tdTomato*$^{+}$ mice and Tomato- cells from CD45.2*Hem1*$^{+/+}$*LysMcre*$^{+}$ control mice, and transferred the cells at a 1:1 ratio IV into CD45.1 host mice. We then administered LPS and assessed the ratio of donor CD45.2 tomato^{-} (WT): CD45.2 tomato^{+} (*Hem1*KO) neutrophils 2 hrs after LPS stimulation in peripheral blood and BALF. Whereas the ratio of WT:*Hem1* KO were unchanged in peripheral blood relative to input, the ratios of WT:Hem-1KO increased in BALF (Figure 7H). These results collectively suggest that Hem-1 is required for neutrophils to migrate appropriately in response to chemokine or LPS stimulation.

To test whether disruption of *Hem1* inhibits the abilities of monocytes to migrate properly, we purified BM monocytes from *Hem1*$^{fl/fl}$*LysMcre*$^{+}$tdTomato^{+} mice and Tomato- cells from *Hem1*$^{+/+}$*LysMcre*$^{+}$ control mice, and transferred the cells at a 1:1 ratio to 5µm pore size transwell plate containing Media or CCL2 chemokine in the lower chamber. We then assessed the ratio of tomato^{-} (WT): tomato^{+} (KO) cell migration 4 hrs after stimulation compared to non-stimulation, then normalized to the control. As expected, *Hem1* null monocytes showed decreased migration towards the chemoattractant (Figure 7I).

Hem1$^{fl/fl}$ LysMcre$^{+/+}$ mice are more sensitive to experimental influenza virus infection.

AMs and epithelial cells are important first-line defense barriers against respiratory viral infections, and PID patients with mutations in *Hem1* present with recurring respiratory infections. Mice with reduced numbers of AMs either from disruption of the *CSF1* gene encoding GM-CSF or myeloid specific disruption of *PPARg* exhibit greatly increased susceptibility to influenza virus infection (21). Because AMs are reduced in *Hem1$^{-/-}$ and Hem1$^{fl/fl}$LysMcre^{+}* mice, we assessed whether myeloid cell specific disruption of Hem-1 alters susceptibility and immune response to experimental influenza virus challenge. We inoculated *Hem1$^{fl/fl}$LysMcre^{++}* and *Hem1$^{+/+}$LysMcre^{++}* control mice with 10 PFU influenza A/PR8 strain or PBS control via oropharyngeal aspiration under anesthesia and measured daily body weight loss for up to 6 days post-infection (DPI) when mice were euthanized, and tissues collected. *Hem1$^{fl/fl}$ LysMcre^{++}* mice exhibited increased daily body weight loss compared to the control mice (Figure 8A), despite equal influenza PFUs in lung tissues (not shown). Analysis of lung sections by H&E revealed dense accumulations of amorphous proteinaceous material, necrotic cells, and nuclear debris in lungs from influenza-infected *Hem1$^{fl/fl}$LysMcre^{++}* mice relative to *Hem1$^{+/+}$* and *LysMcre^{++}* control mice (Figure 8B). PBS control *Hem1$^{fl/fl}$* and *LysMcre+* control mice showed minimal or no lesions (not shown). Analyses of BAL fluid collected at D3 and D6 PI indicated that infection of *Hem1$^{fl/fl}$LysMcre^{++}* mice with influenza resulted in significant increases in optical density of BAL fluid relative to PBS infected or naïve *Hem1$^{fl/fl}$ LysMcre^{++}* mice (Figure 8C). The increase in OD correlated with increased total protein (Fig. 8D) and expression of the epithelial cell marker EpCAM, as well as the endothelial and inflammatory cell marker CD31 (Fig. 8E), suggesting that at least some of the cellular debris in BAL fluid from *Hem1$^{fl/fl}$LysMcre^{++}* mice are derived from epithelial and inflammatory cells.

Total WBC numbers were increased in both *Hem1*$^{fl/fl}$*LysMcre*$^{++}$ and *LysMcre*$^{++}$ mice 6 DPI, which consisted mostly of neutrophils. Interestingly, eosinophil numbers increased and the percentage of CD8T cells were decreased in *Hem1*$^{fl/fl}$*LysMcre*$^{++}$ relative to *Hem1*$^{+/+}$*LysMcre*$^{++}$ mice (Figure 8F). Analysis of BAL fluids revealed that loss of myeloid specific disruption of Hem-1 results in significantly increased concentrations of the proinflammatory cytokines G-CSF, KC, MCP-1, and MIP-1α compared to the *Hem1*$^{fl/fl}$ controls (Figure 8G) which corresponds to massive recruitment of myeloid cells into damaged areas of lung parenchyma. These results indicated *Hem1*-deficient myeloid cells contribute to immunopathological inflammation during influenza virus infection.

Hem1*$^{fl/fl}$ *LysMcre*$^{+/+}$ *BMDMs produce more proinflammatory cytokines upon LPS stimulation. Because we found increased proinflammatory cytokines in *Hem1*$^{fl/fl}$ *LysMcre*$^{+/+}$ BALF relative to *LysMcre*$^{+/+}$ BALF after influenza infection, we next addressed whether these differences could be directly attributed to loss of *Hem1* in myeloid cells. Pro- and anti-inflammatory signaling in response to LPS signaling is regulated by downregulation of the TLR4 receptor and NFκB signaling from a Myd88 directed pathway to a TRIF/TRAM directed pathway to mTOR/Mapk, which drives expression of the anti-inflammatory cytokes IFN-β and IL-10 (22). We first isolated BMDMs and then stimulated the cells with LPS in vitro for 24 hrs. We then measured cytokine expression by a 31-plex cytokine array (Eve Technologies) to test cytokine protein in supernatants. We found that *Hem1* null BMDMs produced more G-CSF, GM-CSF, KC, MIP2, IL-6, LIF, and VEGF (Figure 9A). Next, we investigated whether this excessive cytokine production results from abnormal downregulation and endocytosis of TLR4 by measuring TLR4 expression on BMDMs surface after LPS stimulation at 30, 60, 120 min. We found that at 2 hrs

Hem1$^{fl/fl}$ *LysMcre*$^{+/+}$ BMDMs exhibit ~10% decrease downregulation (Figure 9B). These results suggest that loss of *Hem1* results in altered differentiation of AM and BMDM towards a more proinflammatory phenotype.

DISCUSSION

Children with Primary Immunodeficiency Disease due to mutations in the *Nckap1l* gene encoding Hem-1 are characterized in part by recurrent upper respiratory tract infections leading to bronchiectasis and cytokine hyperresponsiveness. However, the molecular and cellular mechanisms of how mutations in *Nckap1l* result in impaired lung immunity are unclear. In this study, we utilized constitutive and myeloid cell specific Hem-1 disruption models in mice to show that loss of Hem-1 results in significant impairment in the development of mature alveolar macrophages from pre-alveolar macrophages shortly after birth. In addition, reduced numbers of Hem-1 deficient AMs correlated the development of pulmonary alveolar proteinosis (PAP) characterized by increased cellular debris, increased total protein levels, lipid laden AMs, and increased pulmonary pro-inflammatory cytokine production, which resulted in increased morbidity associated with experimental influenza infection. These results collectively suggest that *Hem1* and the WAVE Regulatory Complex (WRC) have critical roles in lung immunity in part by regulating the development and functions of AMs. Our studies provide a myeloid cell specific mechanism of how non-coding or loss-of-function mutations in Hem-1 result in primary immunodeficiency disease and increased susceptibility to respiratory infections. Furthermore, our studies suggest that PID patients with mutations in *Hem1* may also suffer from PAP, which further impairs blood oxygenation and lung immunity.

Alveolar macrophages are important in the defense against viral, bacterial, and fungal infections, while also limiting acute lung injury following infection-mediated damage (23). AMs also have important non-immune functions including clearance of surfactant and apoptotic cellular debris. AMs have potent phagocytic ability, and are important in clearing bacterial and fungal infections, including *Streptococcus pneumonia*, *Mycobacteria tuberculosis*, and

Pneumocystis carinii. AMs have also been shown important roles in reducing morbidity associated with viral infections such as influenza virus (24)(25), in part through production of Type I interferon (26) and clearance of inflammation stimulating dead cells. For example, *Csf2*$^{-/-}$ mice lacking AM due to the absence of GM-CSF exhibit fatal hypoxia, impaired gas exchange, and high morbidity following influenza virus infection (21). Similarly, myeloid-specific *PPARg* deficient mice with defective AMs but normal adaptive immunity, presented with lung failure and increased morbidity to influenza virus(21). Interestingly, *Csf2*$^{-/-}$ mice also exhibited a massive accumulation of dead CD45-negative cells in the BAL and lung consistent with an important role for AM in the removal of dead cells (efferocytosis). In this study, we found that myeloid cell specific disruption of *Hem1* results in a significant reduction of AMs, and increased morbidity (as defined by weight loss and mortality) associated with influenza virus infections. In addition, we found massive accumulations of dead CD45-negative cells that stained positive for Epcam and CD31, which are markers of epithelial cells and endothelial/inflammatory cells respectively, in BALF in uninfected *Hem1*$^{-/-}$ and *Hem1*$^{fl/fl}$*LysMcre* mice. Optical density of BALF further increased in *Hem1*$^{fl/fl}$*LysMcre* mice following influenza infection, suggesting that the accumulation of necrotic debris and dead cells worsened with infection. One difference between *Csf2*$^{-/-}$ mice and *Hem1*$^{fl/fl}$*LysMcre* mice is the absence of neutrophils accumulation in BALF following disruption of *Hem1*. This is likely because neutrophil migration is also impaired following disruption of *Hem1*, whereas neutrophil migration proceeds normally in the absence of *Csf2*. Collectively, our data suggest that Hem-1, in part via induction of protective AMs, is important for efferocytosis, clearance of surfactant, and maintenance of effective lung immunity in response to respiratory infections with influenza virus.

Whereas AMs are important for defense against respiratory pathogens, they also been shown to be important for limiting excessive immune responses following acute infection through the inhibition of DC-mediated activation of T cells and by production of TGF beta, which stimulates regulatory T cell production and acts in an autocrine manner to enhance AM differentiation (27). In addition, AMs inhibit recruitment of neutrophils as well as production of pro-inflammatory cytokines (28). Indeed, we found increased production of the growth factor G-CSF (which stimulates neutrophil production in the BM), the neutrophil chemotactic cytokine KC (CXCL1), the monocyte chemoattractant MCP-1 (CCL2), and the macrophage inflammatory protein MIP-1a (CCL3), in BAL fluid from *Hem1$^{fl/fl}$LysMcre* mice relative to control mice 6 days following influenza infection. Expression of KC, MCP-1, and MIP-1α mRNA were also increased in purified AMs from *Hem1$^{fl/fl}$LysMcre* relative to control mice, and lung inflammation was more severe in *Hem1$^{fl/fl}$LysMcre* relative to control mice as determined by lung histology and immunohistochemistry. These results suggest that Hem-1 may also limit excessive inflammation in response to acute infection, in part by regulating the production of AMs, and/or the switch from "tolerogenic AMs" to "inflammatory AMs" in response to pathogens.

Because we found reduced numbers of AMs in *Hem1$^{-/-}$* and *Hem1$^{fl/fl}$LysMcre* mice, we addressed whether *Hem1* could be important for the development of AMs. The current dogma is that AMs uniquely develop during embryogenesis, whereby embryonic precursors seed lung tissue *in utero* and mature locally shortly before and soon after birth (see(23) for review). In particular, fetal monocytes derived from yolk sac precursors in the fetal liver migrate(29)(20) to the lungs via the bloodstream around embryonic day 15. In response to GM-CSF production by alveolar epithelial cells, fetal monocytes upregulate the nuclear receptor PPARγ, which "instructs" pre-AM differentiation denoted by downregulation of Ly6C and upregulation of

CD11c. Around the time of birth, continued production of GMCSF and PPARγ, in combination with B lymphoid transcriptional repressor Bach2, stimulate further maturation of pre-AMs to mature AMs, characterized by further downregulation of CD11b and Ly6C, and upregulation F4/80, CD11c, SiglecF, and CD64. Importantly, PPARγ controls the intrinsic transcriptional program required for AM function, including cholesterol metabolism, lipid transport and storage, and fatty acid oxidation (30), whereas Bach2 controls expression of the ABCA1 and ABCG1 transporters which are responsible for efflux of excess cholesterol. Mice with prenatal targeted deletion of *Csf2* or *Csf2rb* encoding GM-CSF or GMCSF receptor (31), *PPARγ* (30), or *Bach2* (32) lack or have reduced numbers of AMs and develop PAP, which contributes to poor blood oxygenation and increased morbidity associated with respiratory infections. Similarly, human patients with PAP express low levels of PPARγ ((33). In this study, we found that constitutive or myeloid cell specific disruption of *Hem1* resulted in a significant reduction of AMs in adult mice, and the remaining AMs were characterized by reduced levels of CD11c and increased levels of CD11b indicated of immaturity. In addition, we found that at PND3 (when AM differentiation is maximal), $Hem1^{-/-}$ and $Hem1^{fl/fl}LysMcre$ mice have reduced percentages and total numbers of mature AMs in lung tissue, whereas fetal monocytes and pre-AMs were represented normally. Analyses of BALF from $Hem1^{fl/fl}LysMcre$ and control mice indicated that GM-CSF was expressed higher levels consistent with a proposed feedback loop (34), whereas PPARγ expression was significantly reduced in purified AMs. These results suggest that either *Hem1* null precursor AMs are unable to upregulate *PPARg* in response to GM-CSF, or that pre-AMs or fetal AMs are unable to migrate to the appropriate regions in the lung where they are exposed to GM-CSF. These results collectively suggest that Hem-1 is required for the development of AMs at the pre-AM to AM stage, in part by regulating the abilities of pre-AMs

to migrate to the appropriate niche. Mice deficient in the actin-bundling protein L-plastin (LPL) were found to be similarly required for the development of AMs at the pre-AM to AM cell transition, in part due to failure to upregulate *PPARg* in response to GM-CSF (20). These results collectively suggest that regulation of the actin cytoskeleton may be critical for AM precursor cells to correctly localize to the regions of alveoli where GM-CSF is produced, perhaps by regulating a combination of migration and adhesion capabilities of monocytes and pre-AMs.

Although the reduction of AMs following constitutive and myeloid cell specific disruption of Hem-1 certainly contributes to impaired lung immunity, we also found alterations in the functions of Hem-1 deficient neutrophils. For example, purified neutrophils from *Hem1$^{fl/fl}$LysMcre* exhibited impaired migration *in vitro* as defined by reduced velocity and distance traveled relative to control neutrophils in response to the chemotactic factor fMLP. *Hem1$^{fl/fl}$LysMcre* neutrophils also failed to accumulate in BALF 2 hrs following oropharyngeal installation of LPS relative to WT control neutrophils, which correlated with greatly increased neutrophil numbers in blood from *Hem1$^{fl/fl}$LysMcre* relative to WT controls. These results collectively suggest that deficient neutrophil migration from the vasculature to bronchioles may also contribute to impaired lung immunity in these mice. *Hem1$^{pt/pt}$* mice with non-coding mutations in *Hem1*, as well as *Hem1$^{-/-}$* mice, exhibit basal neutrophilia, which was also associated with increased granulopoiesis in the BM as is seen in *Hem1$^{fl/fl}$LysMcre* mice. Serum levels of IL-17 were increased in *Hem1$^{pt/pt}$* mice, and G-CSF levels were increased in BALF from *Hem1$^{fl/fl}$LysMcre* mice 6 days post influenza infection. Because IL-17 potently stimulates the expansion and chemotaxis of neutrophils in a G-CSF dependent manner, these results suggest that the neutrophilic response may be due in part to reduced neutrophil migration into tissues,

resulting in increased IL-23 production from tissue macrophages and increased T_H-17 cell differentiation (35).

Humans and mice with loss of function mutations in *Hem1* similarly present with defects in multiple immune cell types including T, B, and NK cells. Neutrophils from human *Hem1* PID patients, *Hem1*$^{pt/pt}$, *Hem1*$^{-/-}$, and *Hem1*$^{fl/fl}$*LysMcre* mice all exhibit defects in neutrophil migration, which likely contributes to bacteremia and recurrent bacterial infections in skin and other tissues. In addition, human *Hem1* PID patients, and *Hem1*$^{pt/pt}$ or $^{-/-}$ mice, also exhibit signs of autoimmunity including cytokine overproduction, atopic and allergic disease, splenomegaly, and immune complex or amyloid deposition in kidney or liver (15). The massive immune dysregulation and production of pro-inflammatory cytokines following constitutive disruption of *Hem1* in people and mice further reinforces the importance of utilizing experimental systems whereby *Hem1* functions can be tested in a cell autonomous manner. In this study, we developed a system to delete *Hem1* in only in myeloid cells, which uncovered a novel role for *Hem1* in the development and functions of AMs. In addition, these studies further corroborate that *Hem1* is important in neutrophil migration in a cell autonomous manner. The utilization of tissue specific disruption models in mice, combined with analyses of *Hem1* PID patient immune cells and CRISPR/Cas9 disruption of *Hem1* in primary immune cells and/or HSCs, will allow detailed understanding of how mutations in *Hem1* result in Primary Immunodeficiency Diseases, and influences susceptibility to pneumonia and other diseases.

MATERIALS AND METHODS

Mice

Generation of conditional Nckap1l (Hem1) knockout mice

Strategies for generating conditional knockout mice have been described previously (36). In brief, the vector NCBI: 105855, ES cell(s), and/or mouse strain used for this research project was generated by the trans-NIH Knock-Out Mouse Project (KOMP) and obtained from the KOMP Repository (Sanger I.D: PG00089_Y_3_F01, www.komp.org). *Hem1* gene-targeted mouse ES cells are produced by electroporating *Hem1floxed* construct into wild-type ES cells. Correct homologous recombination between the genome of the ES cell and the two regions of homology where the replacement of the targeted locus with the targeting construct occurs was confirmed by PCR amplification strategy and Southern blot from genomic DNA isolated from targeted ES cells under antibiotic selection. Primers for PCR and probe for Southern blot are listed in Table 1. To generate conditional *Hem1* knockout mice for myeloid cell lineage, *Hem1 floxed* mice were bred to myeloid specific Cre system, transgenic *LysMcre* mice (37) (obtained from Jackson Lab). Moreover, to evaluate *Hem1* deletion efficacy, *Hem1 floxed* mice were also bred to *tdTomato* mice (B6.Cg-*Gt(ROSA)26Sor*$^{tm9(CAG\text{-}tdTomato)Hze}$/J, obtained from Jackson Lab). Mice were bred and maintained in individually ventilated cages at the University of Washington in a specific pathogen-free animal facility. All procedures on mice were reviewed and approved by Institutional Animal Care and Use Committee of the University of Washington.

Polymerase chain reaction (PCR)

Genomic DNA from BMDMs and BM neutrophils were isolated using extraction solution, tissue preparation solution, and neutralization solution (Sigma-Aldrich). Primers for PCR amplification

are listed in Supplemental Table I. PCR was carried out using the EmeraldAmp® GT PCR Master Mix (Takara, Japan). PCR conditions were as follow: 1 cycle of 3 min at 94°C, followed by 35 cycles of 30 sec at 94°C, 50 sec at 55°C, and 50 sec at 72°C, and extension with 7 min incubation at 72°C. The PCR products were run on 3% agarose gel containing 0.0025% ethidium bromide. The gel was imaged by Gel Documentation System (Bio-rad).

Western blot analysis

Western blot analysis was performed as described previously (38). Bone marrow derived macrophages (BMDMs) and MACS-sorted (Miltenyi Biotec) Gr1+ BM neutrophils were isolated from Wt and *Hem1*$^{fl/fl}$*LysMcre*$^{+}$ mice. To test the presence of *Hem1* and *Hem1* complex components, the following Abs were used: *Hem1* (gift from O.D. Weiner, University of California, San Francisco, CA), WAVE2, Abi1, Abi2, and Sra1 (15), (14). GAPDH was used as a loading control Densitometry analysis was performed using ImageJ software.

Flow cytometry

BM cells, splenocytes, blood cells, peritoneal cells, and bronchoalveolar lavage cells were pre-incubated with purified anti-CD16/32 antibody for 10 minutes on ice to block Fc receptors and stained with various fluorescent-conjugated antibodies: B220 (RA3-6B2), CD11b (M1/70), Gr1 (RB6-8C5), CXCR4 (L276F12), cKit (2B8), CXCR2 (SA044G4), Ly6G (1A8), Ly6C (HK1.4), F4/80 (BM8), CD64 (X54-5/7.1), MHC class II (M5/114.15.2), CD11c (N418), Siglec F (S17007L), CD103 (2E7), CD24 (M1/69). Subsets of Myeloid cells were identified based on cell surface markers; leukocytes (CD45.2+), alveolar macrophages (AM) (CD11c^{+}SiglecF^{+}CD64^{+}) neutrophils (CD11b^{+}Ly6G^{+}), eosinophils (SiglecF^{+}CD11c^{-}Ly6G^{-}), CD103^{+} dendritic cells

(DCs) (SiglecF^{-}CD11b^{int} CD24^{+}CD11c^{+}). Flow cytometric data were acquired on a FACS Canto II or LSR II flow cytometer (BD Biosciences), and data were analyzed using FlowJo software.

Analysis of developmental neutrophil lineage and subsets of monocyte/macrophage

Bone marrow, spleen, blood, liver, BALF and lung were collected from 5-10 *Hem1$^{fl/fl}$ LysMcre^{-}* and *5-10 Hem1$^{fl/fl}$ LysMcre^{+}* 6-10 weeks old mice. Cells were subjected to ACK lysis buffer to lysed RBC and resuspended in 3% newborn calf serum/PBS, followed by staining with fluorescent-conjugated antibodies. For gating strategy, B220+ B cells were excluded from analysis, and percentage of myeloid cells are shown within CD11b^{+} Gr1^{+} cells. PreNeu were gated within CXCR4^{+} cKit^{+}, then immature and mature neutrophils were gated by Ly6G^{+} CXCR2^{-} and Ly6G^{+} CXCR2^{+}, respectively. Neutrophil development was assessed as described in (39). Monocytes and macrophages were gated on CD11b^{+}F4/80^{+}Gr1^{+}.

For AMs development analysis, alveolar macrophages were identified based on CD11c^{+}SiglecF^{+}CD64^{+}CD11b^{-}, after excluding B cells, neutrophils and dendritic cells marked with B220^{+}, Ly6G^{+} and CD11c^{+}, respectively (7). Pre-AMs were identified by CD11c^{int}CD11b^{int}Sigleg-F^{int} (40), Fetal monocytes and macrophages were identified by F4/80^{int}CD11b^{hi}CD11c^{lo}Ly6C^{hi} and F4/80^{hi}CD11b^{int}CD11c^{lo} respectively.

Bronchoalveolar lavage fluid analysis

BALF was aliquoted and measured turbidity by spectrophotometer with 590 nm wavelength. 100µl of BALF was cytospin and stained with Diff-Quik, Oil red O and PAS. Alveolar macrophage sizes were analyzed by mean FSC-A using flow cytometry. Leukocytes and

epithelial cells were stained with fluorescent CD45.2 and EpCAM (CD326) antibody respectively and analyzed by flow cytometry.

Oil red O staining

BALF 100 ul was cytospin, air dry and fix in 10% formalin, wash twice in distill water, then 60% isopropyl alcohol followed by oil red O 15 min, wash twice in distill waster. The nuclei were stained with DAPI and mounted with mounting buffer.

Total protein measurement

Total protein contents from BALF supernatant were determined by spectrophotometer at OD 590 using Bradford assay (41)

Alveolar macrophage development

Timed breedings were set up to harvest neonatal day3 pups. Lungs and liver were harvested from mice and incubated 30 min at 37°C in digestive enzyme (DNase and Collagenase IV), then stained with appropriate antibodies and analyzed by flow cytometry.

F-actin polymerization assay

F-actin assay was described previously (15). Bone marrow cells isolated were plated on 96-well plate, and then were stimulated with 1uM fMLP for 2 minutes. Cells were fixed, permeabilized and intracellularly stained with FITC-Phalloidin in conjunction with fluorescent conjugated anti mouse CD11b and anti-mouse Ly6G (9). Intensities of F-actin polymerization were measured by flow cytometry or imaged by fluorescence microscope after preparing cytospin slide.

Generating Bone marrow derived macrophages

Total bone marrow cells collected were cultured with supplemented L929-supernatant media for 7-10 days to generate bone marrow-derived macrophages (BMDMs). The purity of BMDMs was >90% based on flow cytometry analysis (48).

In vitro phagocytosis assay

BMDMs were fed with 1μm fluorescent beads (MOI 30) for 1 hour at 4°C and 37°C. The cells were washed 3 times to remove extracellular beads, then stained with fluorescent antibody F4/80 and analyzed by flow cytometry.

In vivo phagocytosis assay: airway neutrophils, alveolar macrophages, and peritoneal macrophages

Mice were introduced with 50ul of LPS (10ug) via oropharyngeal aspiration under isoflurane anesthesia to recruit neutrophils into lavage fluids. 2 hr later, fluorescent beads were given to the mice via the same route as described above. 30 min later, the mice were euthanized by cervical dislocation and BALF was collected. The cells were stained with fluorescent conjugated antibodies with anti CD45.2, anti Ly6G, and anti CD64. Percent phagocytosis was analyzed by flow cytometry. *in vivo* peritoneal macrophages phagocytosis assay, 10^7 FITC-labeled beads were injected into the peritoneal cavity. The mice were euthanized one hour later, and peritoneal fluid was collected using 3 ml of ice-cold PBS/3%FBS. Cells were stained with anti-F4/80-APC Ab on ice 30 min. The percentage of peritoneal macrophages phagocytosis was determined by flow cytometry (49).

Isolation of murine bone marrow neutrophils

Bone marrow cells were harvested from *Hem1$^{fl/fl}$ LysMcre^{+}* and *Hem1 $^{fl/fl}$ LysMcre^{-}* or *Hem1$^{fl/+}$ LysMcre^{-}* mice. The RBCs were lysed with 0.2% NaCl for 45 sec and restored osmolarity with 1.2% NaCl before passed through a 70 micron cell strainer. Neutrophils were further purified by 62% Percoll. The purity of neutrophils was >90% based on flow cytometry analysis.

2D Neutrophil Chemotaxis assay

Chemotaxis assay was performed as previously described (42),(43). Briefly, the 6 ul of 3 x 10^6 cells/ml neutrophils were allowed for 20 min. to adhere to the cell channel connecting the two 60 ul reservoirs of the µ-slide chemotaxis (Ibidi Cat. No. 80326, Germany). Two reservoirs were gently filled with 60 ul medium and one side of reservoir was loaded with 30 ul LTB4 which reaches the final concentration 1uM LTB4 after diffused in the reservoir. Cells on micro-slide was imaged by phase-contrast microscopy via a 10x objective lens. Images were captured every 1 min for 1 hour, and cell migration tracks were analyzed with ImageJ (National Institute of Health) using a manual track plugin and the chemotaxis and migration tools from Ibidi. Forty randomly selected neutrophils were manually tracked in each chemotaxis experiment. T y-forward migration index (FMI), directness, distance, velocity was the metrics used as chemotactic efficiency. Cell viability was measure by DeadSytox staining and analyzed by flow cytometry.

In vivo neutrophil migration assays

LPS-induced model was described previously (44), (45). Mice were aspirating with 10ug LPS O111:B4 after anesthetized with isoflurane. Three hours later, mice were bled and euthanized by

cervical dislocation to collect bronchoalveolar lavage fluid (BALF) (46). Migrated cells into lavage fluids were stained with fluorescent conjugated anti CD45.2 and anti Ly6G and analyzed by flow cytometry. Total number of cells were determined using hemocytometer cell counting method.

In vivo competitive neutrophil migration assay

BM Neutrophils were isolated from *tdtomato*$^{-}$ WT and *tdtomato*$^{+}$ *Hem1*$^{fl/fl}$ *LysMcre*$^{+}$, then mixed 1:1 ratio and injected via i.v. to CD45.1 recipient mouse. The recipient mice were instilled with LPS via o.p. to recruit immune cells. The mice were euthanized 2 hours later to collect BALF and blood and stained with CD45.2, Ly6G and analyzed by flow cytometry.

In vitro competitive monocyte migration assay

BM monocytes were isolated from *tdTomato*$^{+}$ *Hem1*$^{fl/fl}$ *LysMcre*$^{++}$ and *tdtomato*$^{-}$ control mice by EasySep™ Mouse Monocyte Isolation Kit. The KO cells were mixed 1:1 ratio with *tdTomato* negative WT cells and plated into 24 transwell insert (5 um pore size) containing CCL2 (vary doses) in the lower chamber. The cells were incubated 4 hours at 37°C in 5%CO_2. The migration ability was analyzed by flow cytometry and normalized to the maximum migration of WT cells (set at 100%) (47).

Influenza A assay

Male *Hem*$^{+/+}$*LysMcre*$^{+/+}$ and *Hem1*$^{fl/fl}$ *LysMcre*$^{+/+}$ mice 6-10 weeks old were anesthetized under isoflurane and inoculated with 10 PFU H1N1 influenza (PR8/A) via oropharyngeal aspiration with 50 ul volume. Mice were monitored daily for changes in body weight, clinical score, and

mortality. At 3- and 6-days post infection (dpi) mice were bled and euthanized. Influenza viral load was quantified with plaque assay performed at Frevert Lab, SLU. In brief, MDCK cells were cultured and seeded 10^6 cells/ well on 12 well plates. A day later, homogenize the virus infected lungs were serially diluted in 10-fold before seeding to the MDCK cells. At 48 hr, cells were fixed with 4% formaldehyde and examined the plaque forming unit and stained with Flu specific Ab. Cellular analysis was performed by staining with fluorescent antibodies and quantified by flow cytometry.

Histochemistry

For histopathology analysis, lungs from naïve, PBS-inoculated and influenza-inoculated mice were harvested. Lungs was perfused and fixed with 10% formalin before harvesting left side of lung. Lungs were stained with hematoxylin and eosin. Lung immunohistochemistry (IHC) was performed with anti Ly6B (neutrophils) and anti CD68 (macrophages) antibodies. Cell infiltration was visualized by NDP view program and semi-quantified by ImageJ.

Cytokine assay

Cytokine levels from BAL supernatants were measured using Multiplex Immunoassay analyzed with a BioPlex 200 Mouse Cytokine Array/ Chemokine Array 32-Plex (MD31, Eve Technologies).

Expression of cytokine/chemokine gene by Realtime PCR

BMDMs or AMs were stimulated with or without LPS for 24 hr. RNA was extracted using RNAqueous-4PCR kit or Micro Total RNA Isolation Kit (Invitrogen Life Technologies). First-

strand cDNA was synthesized from RNA using reverse transcriptase (Superscript III; Invitrogen Life Technologies). The cDNA was amplified by quantitative real-time PCR using Power SYBR® Green PCR Master Mix (Fisher Scientific Company). Thermal cycling was initiated with a first denaturation step of 5 min at 95°C, followed by 40 cycles of 95°C for 10 s and 60°C for 30 s. The fluorescence emitted from amplified DNA was read at 60°C at the end of each cycle. The data of the real-time PCR amplification were analyzed using the iCycler iQ and the Real-Time PCR Optical System Software version 3.0 (Bio-Rad). The cycle number at which the various transcripts were detectable, referred to as the threshold cycle (Ct), was compared with that of β-actin and referred to as ΔCt. The relative gene level was expressed as $2^{-(\Delta\Delta Ct)}$, in which ΔΔCt equals ΔCt of the experimental sample minus ΔCt of the control sample. The specific primers were provided in Table1.

TLR4 expression assay

BMDMs or AMs were stimulated with LPS in indicating timepoints and stained with TLR4 antibody then analyzed percentages of mean fluorescent intensity by flow cytometry (52).

Statistical analysis

All statistical analysis was performed using GraphPad Prism software. Statistical differences were determined using the Student *t* test with Holm-Sidak correction for multiple comparison or two-way ANOVA. All data are presented as mean± SEM.

FIGURES

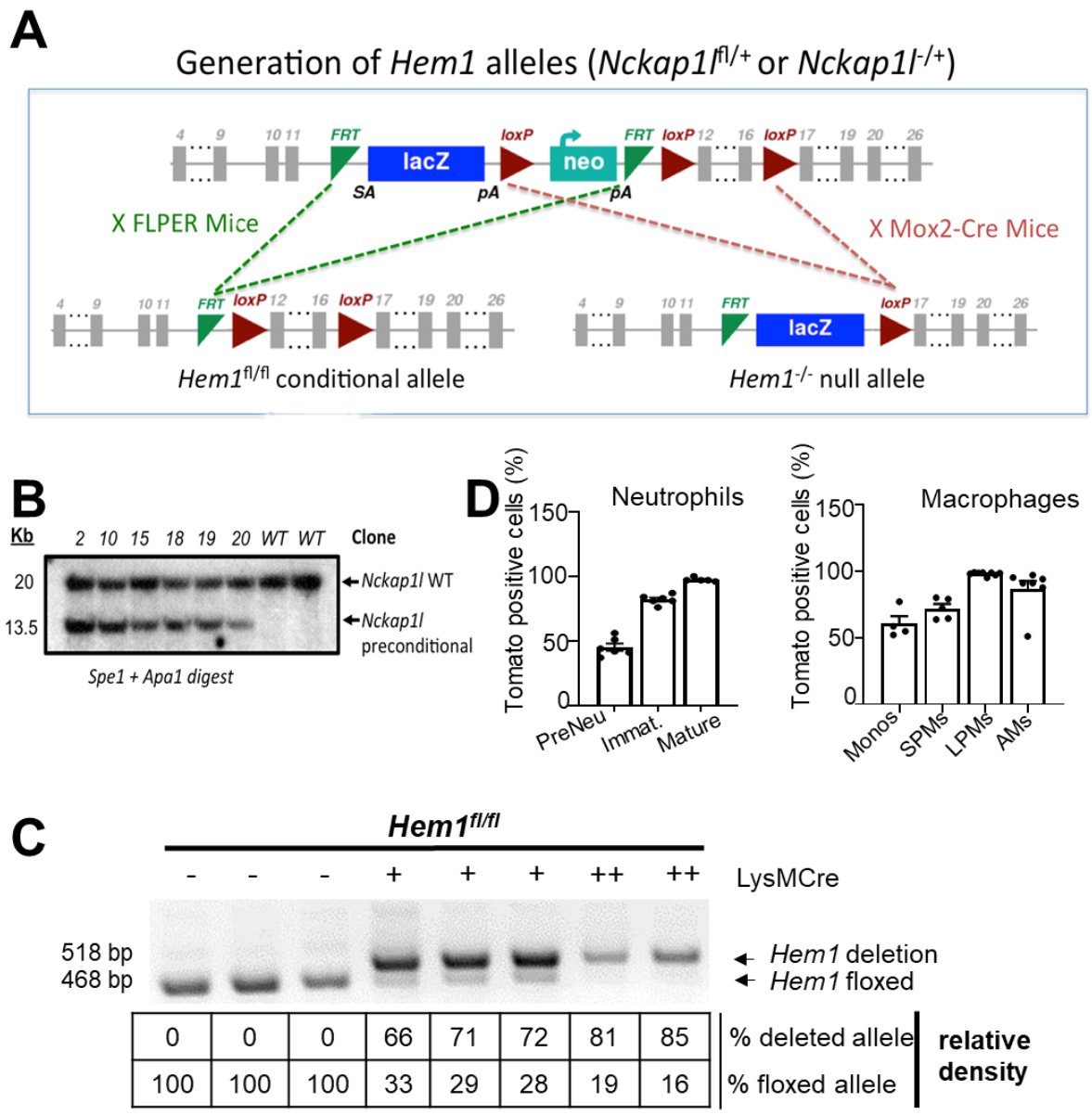

0	0	0	66	71	72	81	85	% deleted allele
100	100	100	33	29	28	19	16	% floxed allele

Figure 1. Generation of *Nckap1l* Null, *Nckap1l floxed*, and Myeloid specific *Hem1* null mice
(A) *Hem1*$^{fl/fl}$ conditional allele mice were generated by flanking the first coding exon of the *Hem1* gene with loxp sites. FLPER mice were bred to delete FRT and Mox2-cre mice were bred to delete *Hem1* gene. (B) 6 clones were tested by southern blot and were confirmed to be correctly targeted to the *Nckap1l* locus (C) PCR analysis of genomic DNA isolated from *Hem1*$^{fl/fl}$ *LysMcre* bone marrow derived macrophages (BMDMs). (D) Percentage of Cre expression in indicated cells from *LysMcre*$^{+}$ *tdTomato* mice.

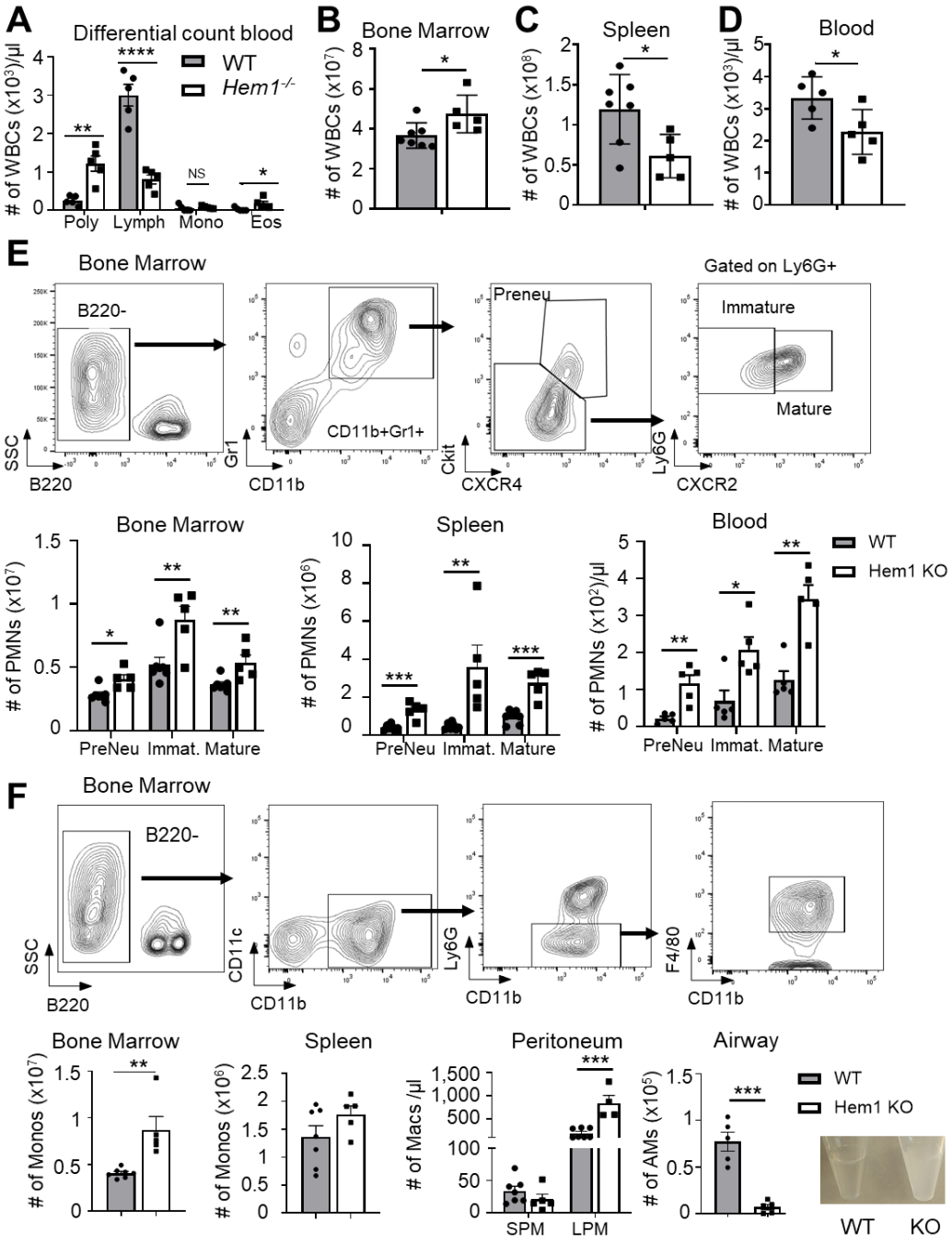

Figure 2. Constitutive disruption of *Hem1* results in increased myelopoiesis, neutrophilia, eosinophilia and lymphopenia. (A-D) Bar graph show the number of WBCs in BM (A), spleen (B), and blood (C-D) from *Hem1*$^{-/-}$ and WT mice. (E) Gating strategy of three different stages of BM neutrophils by flow cytometry. Bar graphs depict Preneu, immature, and mature neutrophil number in BM, spleen, and blood. (F) Gating strategy of BM monocytes by flow cytometry. Bar graphs depict monocytes/macrophages number in BM, spleen, peritoneum, and airway, and BALF appearance. Shown data are mean±SEM from 5-7 mice/genotype. *p<0.05 **p<0.01 ***p<0.001 by Student's two-tailed t-test.

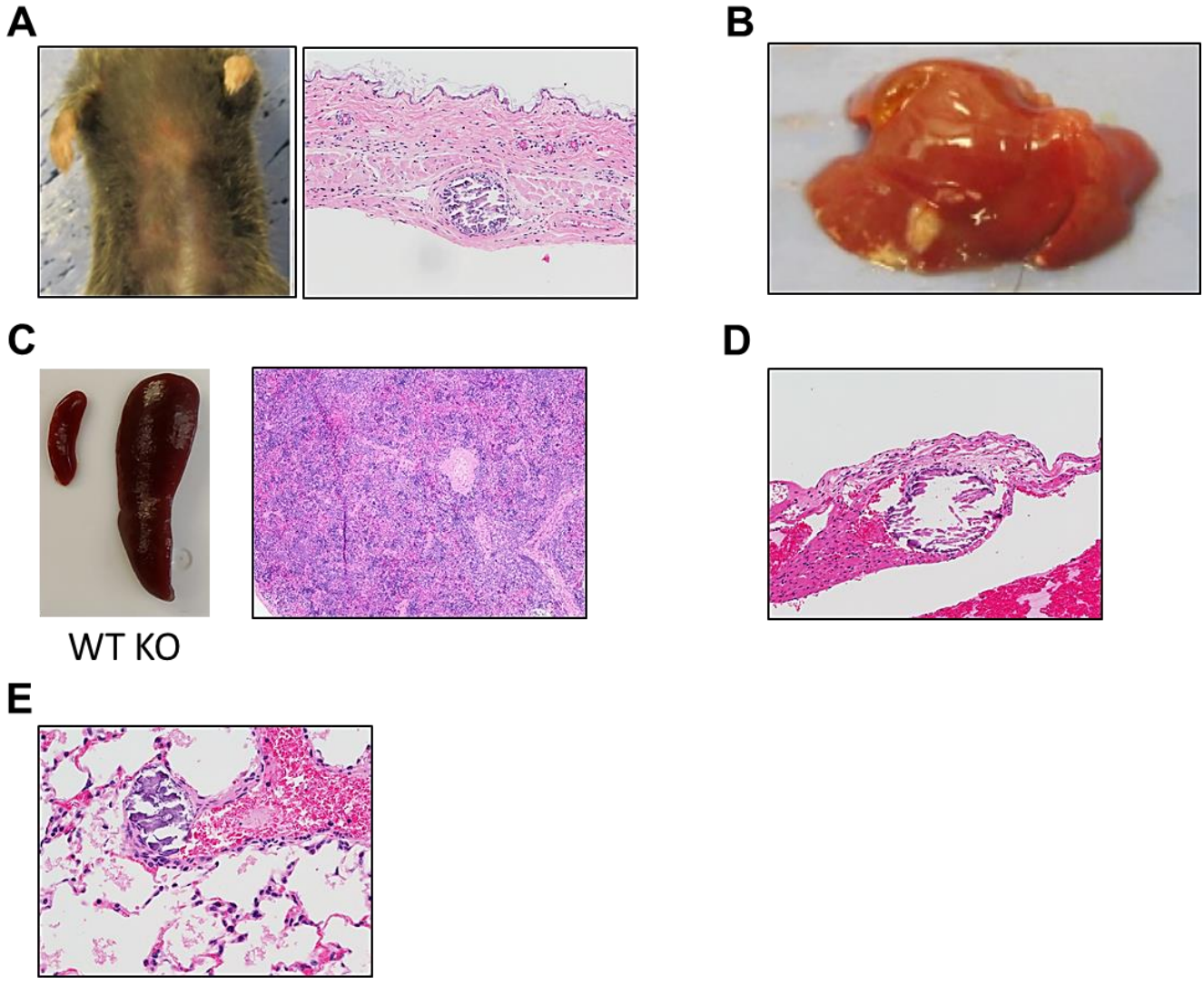

Figure 3 Constitutive disruption of *Hem1* results in alopecia, extramedullary hematopoiesis, and internal organ mineralization. (A) A linear line of alopecia and thickened dermis approximately 1.5cm x 0.3cm present on the abdomen extending from the thorax to the prepuce. The skin on the margins is reddened. Multifocal mild mineralization and hemorrhage within the dermis (B) Multiple well demarcated white discolorations are present on the margins of the liver on multiple lobes. Multifocal mild mineralization and fibrosis (C) The spleen is approximately 3x normal size (splenomegaly). Extramedullary hematopoiesis with moderate diffuse lymphoid depletion. (D) There are multiple white well demarcated foci on the margins of the auricles of the heart bilaterally. Heart Auricles: Mild to moderate multifocal to coalescing white discolorations, chronic-active with mild mineralization (E) The lungs are mildly consolidated in appearance. Appearance of a fissure line was present on the caudal aspect of the left lung lobe; the margins of this lesion are rounded (not shown). Multifocal mild vessel mineralization.

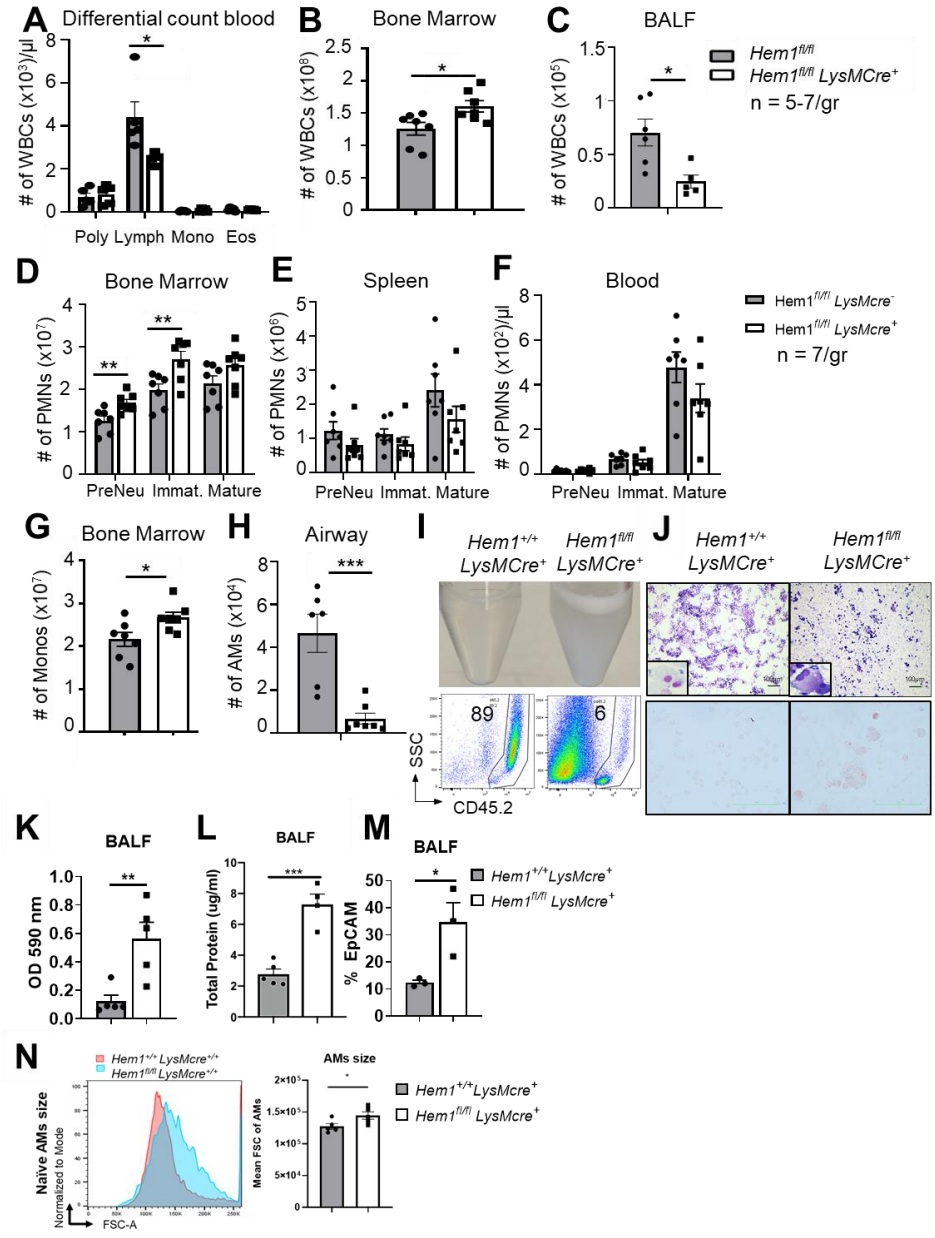

Figure 4 Myeloid specific disruption of *Hem1* results in lymphopenia, increased myelopoiesis, and decreased alveolar macrophages number. (A-C) Bar graphs show WBCs number in blood (A), BM (B), BALF (C) from *Hem1$^{fl/fl}$ LysMcre^{+}* and littermate control. (D-F) Absolute number of PMNs three stages in BM (D), spleen (E), and blood (F). (G) Number of monocytes BM. (H) Absolute number of AMs in airway. (I) BALF appearance, CD45.2 and Side Scatter of BALF by flow cytometry. (J) BALF cytospin with Diff-quik staining and oil red O (K) BALF turbidity measured by spectrophotometer. (L) Total protein in BALF measured by Bradford assay. (M) Precent EpCAM in BALF (N) Size of AMs shown in Forward Scatter-A by flow cytometry. Bar graph shows mean FSC of AMs. Shown data are mean+/- SEM from 4-7 mice/genotype. *p<0.05 **p<0.01 ***p<0.001 ****p<0.0001by Student's two-tailed t-test.

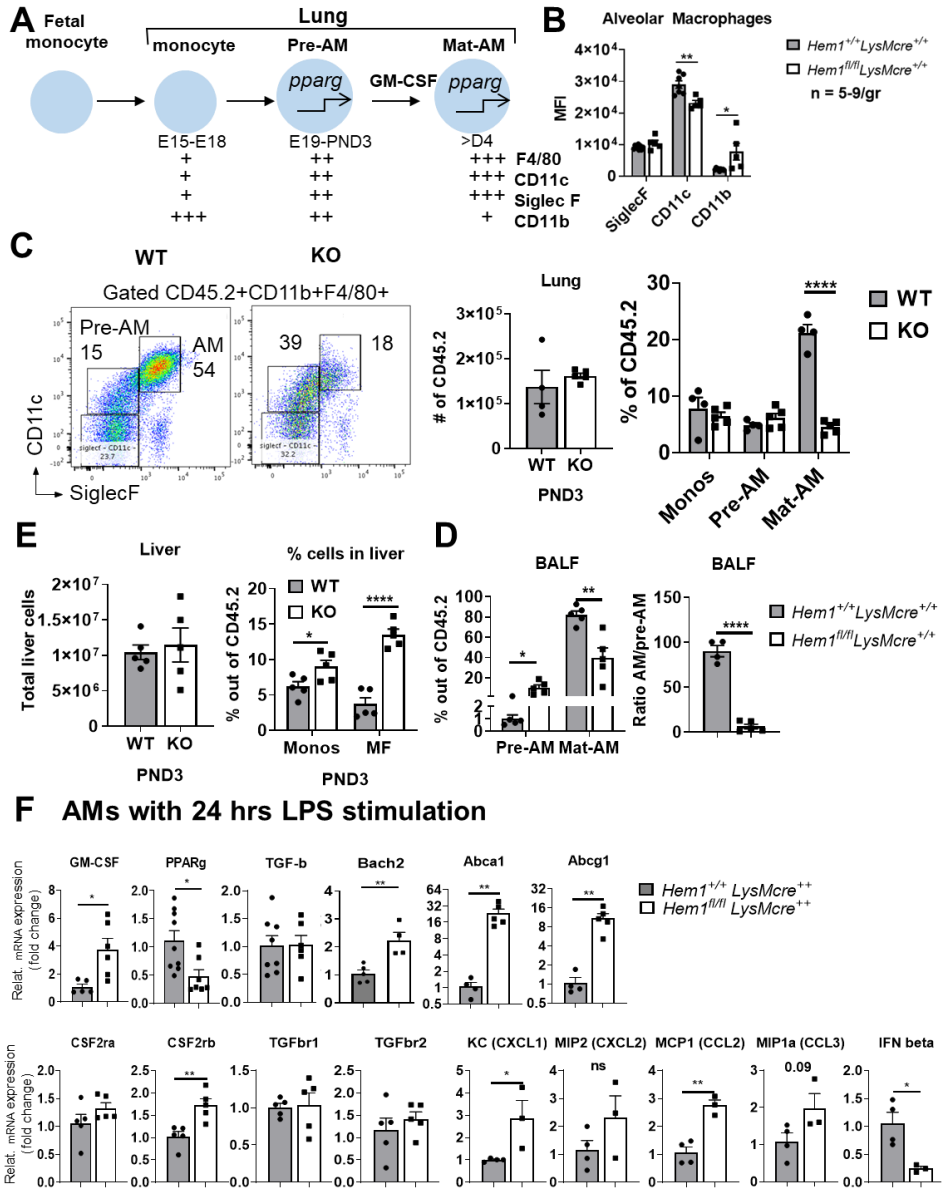

Figure 5 *Hem1* is required for the development of alveolar macrophages from pre-alveolar macrophages. (A) Diagram shows AMs development from monocytes, pre-alveolar macrophages (pre-AM), and mature alveolar macrophages (mat-AM) with cytokine regulation and surface marker expressions in each stage. (B) Mean fluorescence intensity (MFI) of surface marker expression in BALF AMs. (C) Dot plot of flow cytometric analysis show pre-AMs and AMs gating strategy and bar graphs show number of WBCs and percentages of indicated cells in lungs from post-natal day 3 (PND3) mice (D) Total WBCs and percentages of cells in PND3 liver. (E) Frequencies of pre-AM amd mature AMs in BALF (left) and ratio Mat-AM/pre-AM (right). (F) Cytokines expression in AMs after 24 hrs LPS stimulation measured by real-time PCR. Shown data are mean+/- SEM from 5 mice/genotype. *p<0.05, **p<0.01, ***p<0.001, ****p<0.0001 by Student's two-tailed t-test.

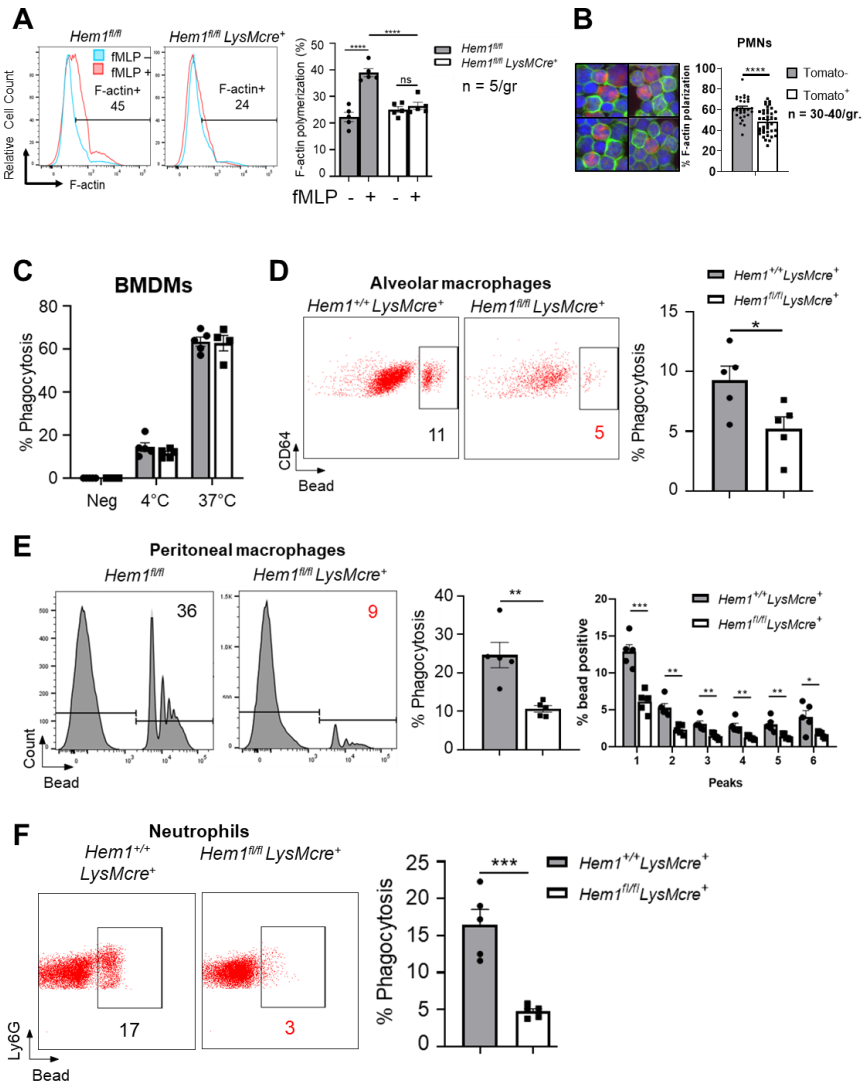

Figure 6. Myeloid specific *Hem1* disruption impairs F-actin polymerization and phagocytosis. (A) Histogram of fluorescence intensity of phalloidin-specific F-actin with and without 1uM fMLP stimulation for 2 minutes in BM PMNs. Bar graph show percentage of F-actin polymerization. (B) Fluorescent imaging of neutrophils from *Hem1*$^{fl/fl}$*LysMcre*$^{+}$ *tdTomato*$^{+}$ mice (red) stained with FITC phalloidin (green) and nuclei staining DAPI (blue) with bar graph showing percentage of F-actin polarization (C) Percent phagocytosis of BMDMs with 1µm bead after 1 hr. (D) Dot plots of flow cytometric analysis show fluorescent bead phagocytosis by CD64^{+}AMs in vivo. Bar graph depicts the percent phagocytosis. (E) Histograms of flow cytometric analysis show microbead phagocytosis by F4/80^{+} peritoneal macrophages. Phagocytosing no beads are in the far-left peak of each panel. Proceeding toward the right of that peak are macrophages phagocytosing 1, 2, 3 or 4 or more beads. Bar graphs show the percentages of macrophages phagocytosing 1 or more beads. (F) Dot plots show neutrophil phagocytosis in vivo after o.p. LPS instillation and fluorescent bead. Bar graph shows percent phagocytosis. (G) MFI of CD11b adhesion molecule in different stages of PMNs. Shown data are mean+/- SEM from 5 mice/genotype. *p<0.05, **p<0.01, ***p<0.001, ****p<0.0001 by Student's two-tailed t-test.

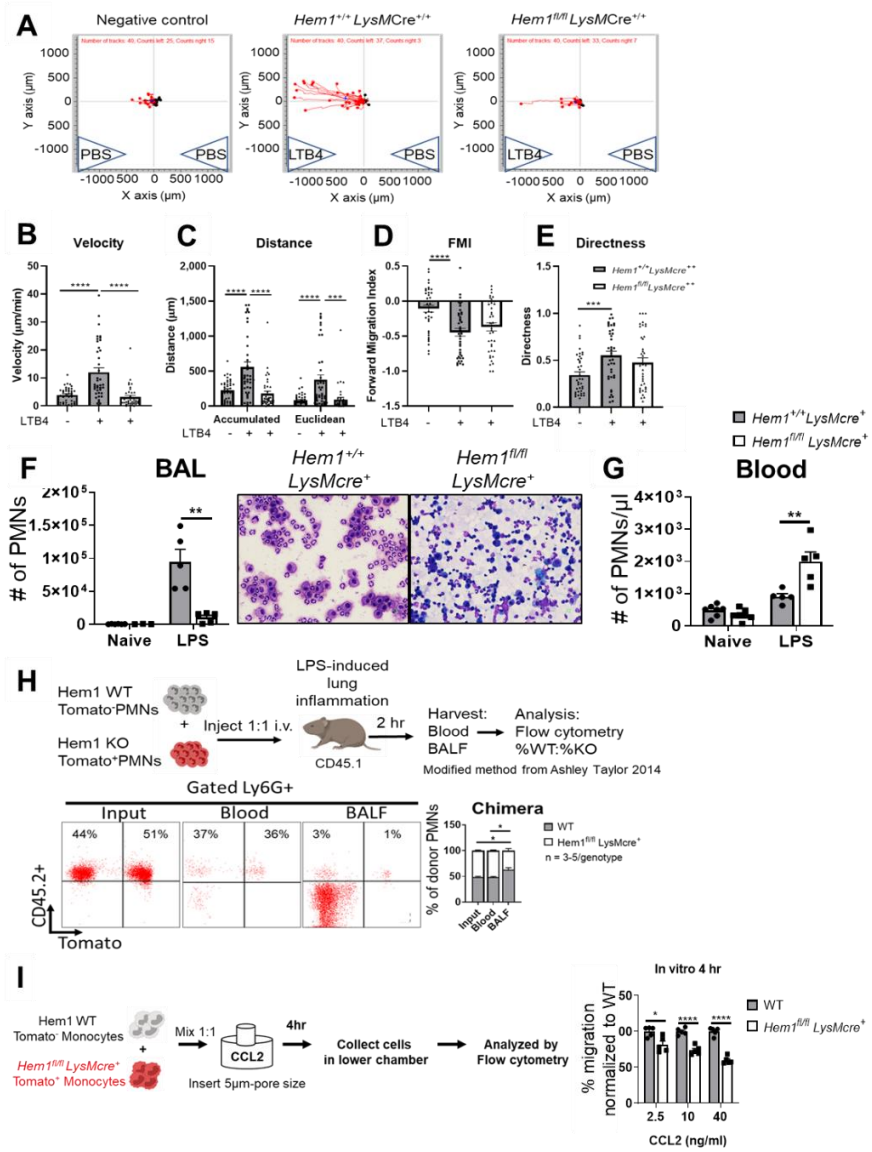

Figure 7. Myeloid specific *Hem1* disruption impairs neutrophil and monocyte migration. (A) Plot migrations of BM neutrophils during 1 hr of LTB4 stimulation (B) Velocity of the migration, (C) Distance of the migration; Accumulated = total distance, Euclidean = straight-line distance between start and stop points (D) Forward Migration Index (FMI). (E) Directness of the migration. (F) Number of neutrophils in BALF before and after LPS instillation 2hrs (left) and cytospin of BALF after LPS stimulation (right). (G) number of PMNs in blood with or without oropharyngeal LPS administration 2 hr. (H) Diagram shows competitive PMNs migration method using Tomato mice. Dot plot show frequencies of cells donor tomato-WT and *Hem1$^{fl/fl}$LysMcre^{+} tdTomato^{+}(*KO) cells in indicated tissues. Bar graph shows percent donor cells normalized to 100% total. (I) Diagram shows competitive Monocytes migration using tomato cells and transwell plate containing CCL2 chemokine different doses. Bar graph shows the percentage of migration normalized to WT. (I) Percent monocytes migration normalized to control. Shown data are mean+/- SEM from 40 cells/genotype. ***p<0.001, ****p<0.0001 by Student's two-tailed t-test

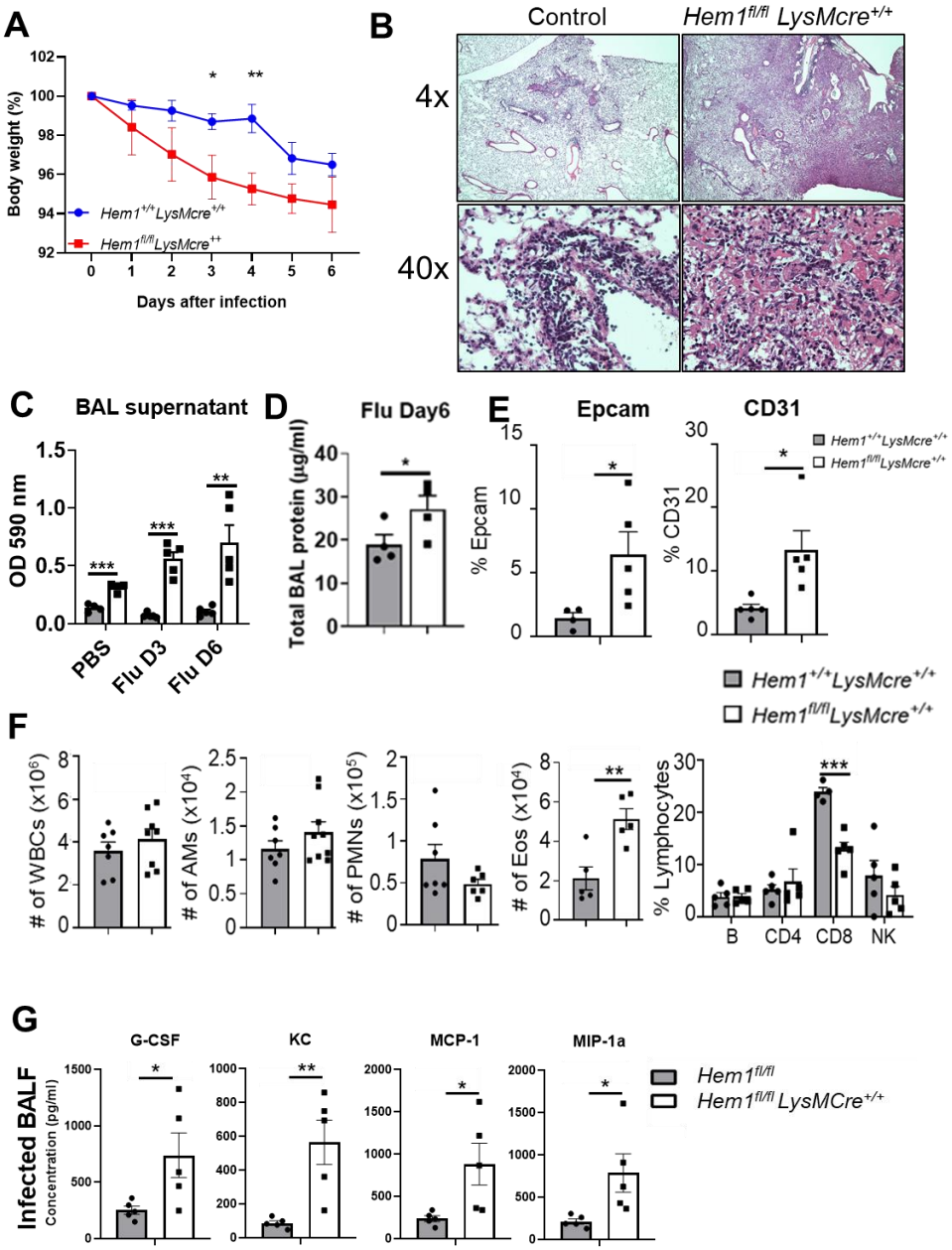

Figure 8. Loss of *Hem1* increases sensitivity to Influenza infection. (A) *Hem1*$^{fl/fl}$ *LysMcre*$^{+/+}$ mice show significantly increase body weight loss in response to influenza A infection compare to control mice (B) H&E staining of lungs after 6 days influenza inoculation. (C) Optical density of BALF indicating turbidity. (D) Total protein in BALF from 6 days influenza infected mice. (E) Percent Epcam and CD31 in BALF at 6 dpi analyzed by flow cytometry (F) Number of cells in BALF at 6dpi (G) Concentrations of cytokines from influenza infected BALF. Shown data are mean+/- SEM from 5 mice/genotype. (*p<0.05,**p<0.01,***p<0.001 by Student's two-tailed t-test.

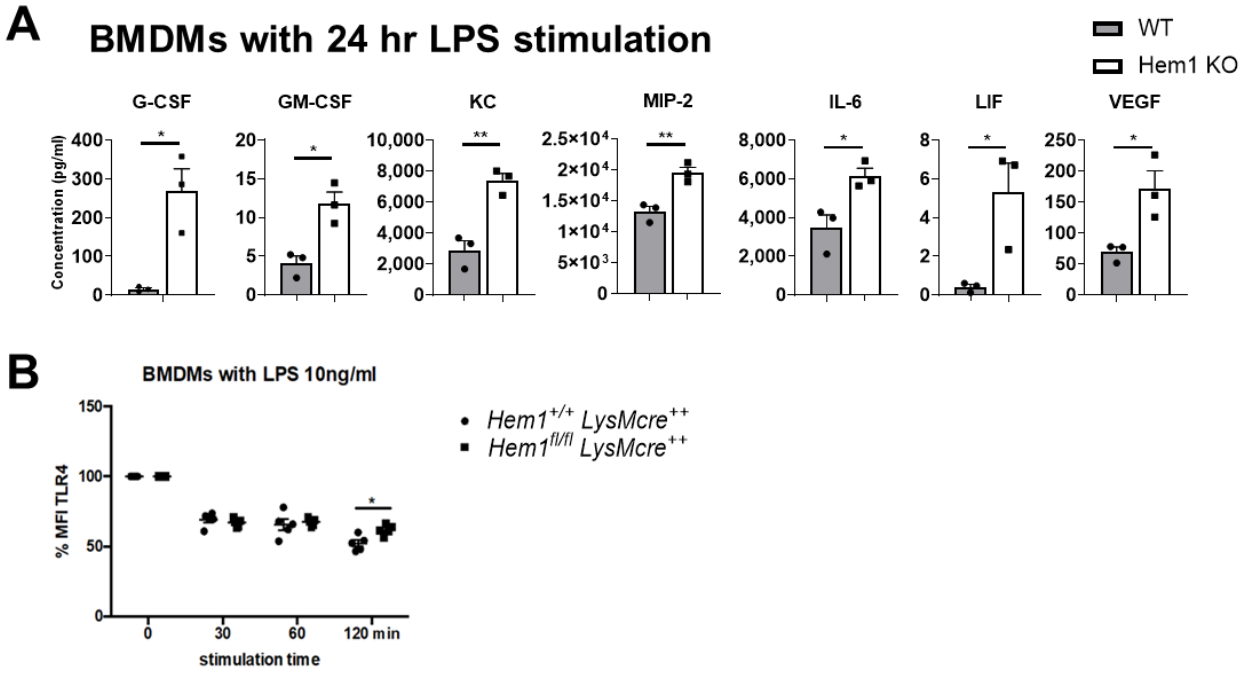

Figure 9. *Hem1* null BMDMs produce more pro-inflammatory cytokines upon LPS stimulation. (A) Bar graphs show concentration of indicated cytokines from Bone marrow-derived macrophages (BMDMs) after 24 hr LPS stimulation. (B) Percent Mean Fluorescent Intensity (MFI) of TLR4 in BMDMs after indicated time of LPS stimulation.

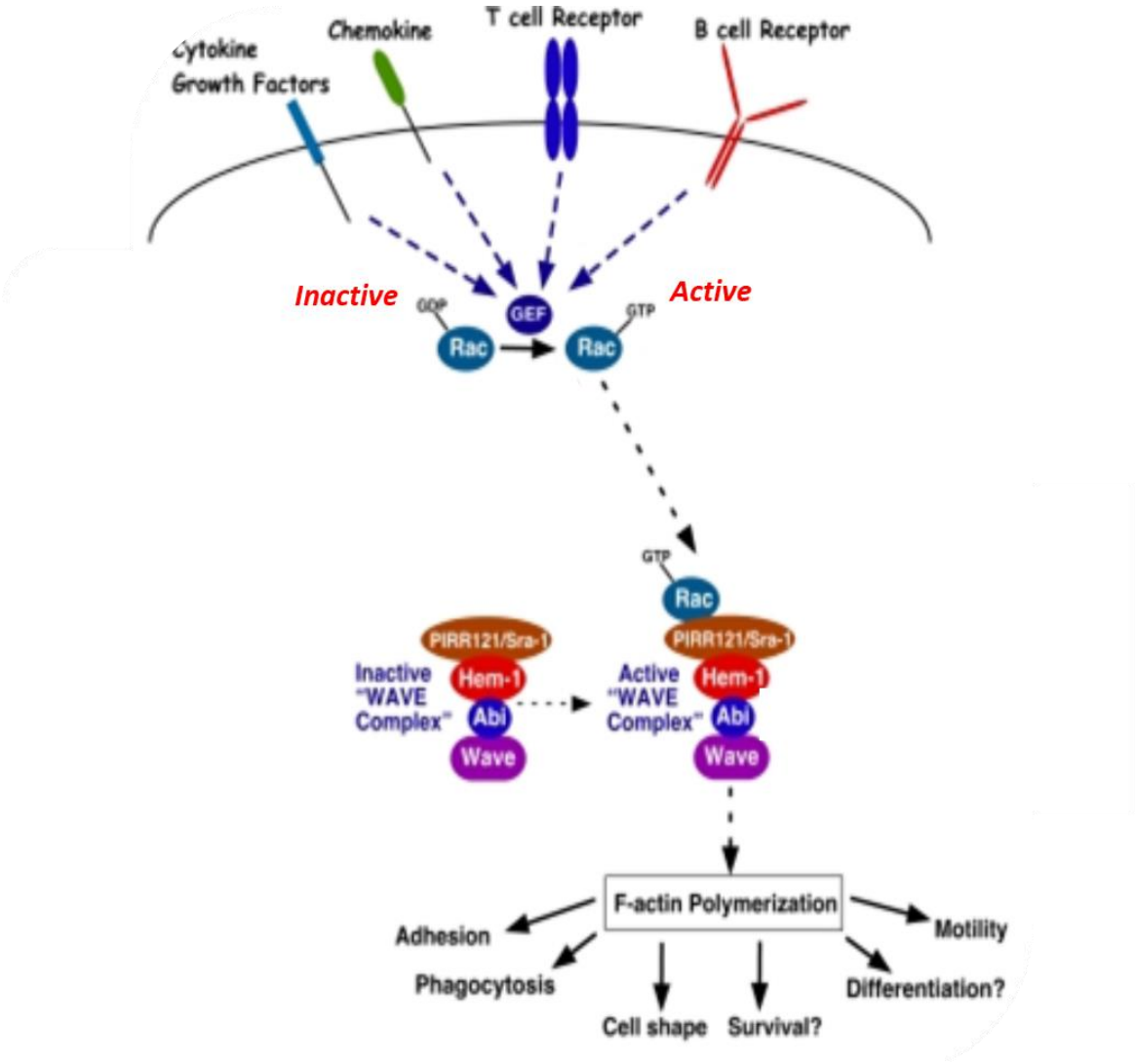

Modified from Park et al., 2008

Figure 10. A model of *Hem1* role in F-actin regulation. Immune cells receive stimuli via receptors on the cell surface. Consequently, Guanine nucleotide exchange factor (GEF) converts Rac-GDP, an inactive form of Rac, to be an active form Rac-GTP. Rac-GTP then activates WAVE complex resulting in F-actin polymerization which is believed to be important for immune cells functions.

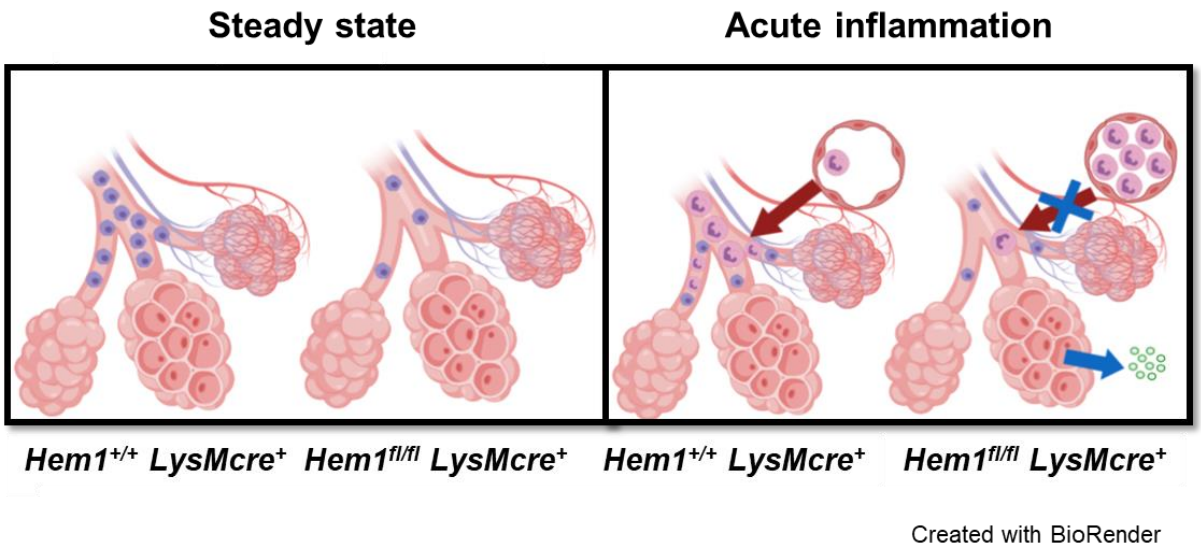

Figure 11. A model of *Hem1* roles in respiratory immunity. In steady state, more than 90% of immune cells in normal airway are alveolar macrophages (AMs), however, disruption of *Hem1* results in decrease number of AMs due in part to developmental defect together with phagocytosis defect leading to increase of debris, protein and surfactant accumulation in the airway, indicating Pulmonary Alveolar Proteinosis (PAP). In acute inflammation state, normal neutrophils can migrate to the airway, however, *Hem1* null neutrophils failed to migrate efficiently from blood vessel to the airway resulting in neutrophilia. Subsequently, immune cells and epithelial cells release cytokines to recruit more neutrophils to the inflammatory site leading to cytokine storm and increase illness.

Table 1

Name	**Primers**
Hem1 floxed FW	CTGGTGTGTCCTGTTTCTGATTTC
Hem1 floxed RW	GTGGCTCACAACTACCTTGTATAAC
LysMcre FW	CTTGGGCTGCCAGAATTTCTC
LysMcre RW1 (WT)	TTACAGTCGGCCAGGCTGAC
LysMcre RW2 (cre)	TCAGCTACACCAGAGACGG
Hem1 deletion FW1	ACCATCTCTCATGCCCCATTCCTG
Hem1 deletion FW2	GCTGGTGGAAACCTCTGACCTTTC
Hem1 deletion RW	CCGAGTACTCATATCAAGTGGCTC
GM CSF FW	TTTACTTTTCCTGGGCATTG
GM CSF RW	TAGCTGGCTGTCATGTTCAA
PPARg FW	TGTGGGGATAAAGCATCAGGC
PPARg RW	CCGGCAGTTAAGATCACACCTAT
TGF beta1 FW	GGAGAGCCCTGGATACCAAC
TGF beta1 RW	CAACCCAGGTCCTTCCTAAA
Bach2 FW	AGTTCATCCACGACATCC
Bach2 RW	AGGTGATTCCTCTCCGAC
KC FW	GGCGCCTATCGCCAATG
KC RW	CTGGATGTTCTTGAGGTGAATCC
MIP-1a FW	ACTGACCTGGAACTGAATGCCTGA
MIP-1a RW	ATGTGGCTACTTGGCAGCAAACAG
MIP-2 FW	ATCCAGAGCTTGAGTGTGACGC
MIP-2 RW	AAGGCAAACTTTTTGACCGCC
MCP-1 FW	CCACTCACCTGCTGCTACTCAT
MCP-1 RW	TGGTGATCCTCTTGTAGCTCTCC
IFN beta FW	CCAGCTCCAAGAAAGGACGA
IFN beta RW	CGCCCTGTAGGTGAGGTTGAT
Abca1 FW	CTCAGTTAAGGCTGCTGCTG
Abca1 RW	TCAGGCGTACAGAGATCAGG
Abcg1 FW	GCCTACTACCTGGCAAAGACC
Abcg1 RW	AGCAGCGAACAGCACAAAAC
CSF2ra FW	CTGCTCTTCTCCACGCTACTG
CSF2ra RW	GAGACTCGCCGGTGTATCC
CSF2rb FW	GTGGAGCGAAGAGTACACTTG
CSF2rb RW	CCAAAGCGAAGGATCAGGAG
TGFbr1 FW	CATTCACCACCGTGTGCCAAATGA
TGFbr1 RW	ACCTGATCCAGACCCTGATGTTGT
TGFbr2 FW	AACGACTTGACCTGTTGCCTGT
TGFbr2 RW	CTTCCGGGGCCATGTATCTT

REFERENCES

1. Dominguez R, Holmes KC. Actin structure and function. *Annu Rev Biophys* 2011;

2. Cook DR, Rossman KL, Der CJ. Rho guanine nucleotide exchange factors: Regulators of Rho GTPase activity in development and disease. *Oncogene* 2014; doi:10.1038/onc.2013.362

3. Cotteret S, Chernoff J. The evolutionary history of effectors downstream of Cdc42 and Rac. *Genome Biol.* 2002; doi:10.1186/gb-2002-3-2-reviews0002

4. Janssen WJM, Geluk HCA, Boes M. F-actin remodeling defects as revealed in primary immunodeficiency disorders. *Clin. Immunol.* 2016; doi:10.1016/j.clim.2016.01.009

5. Lemahieu V, Gastier JM, Francke U. Novel mutations in the Wiskott-Aldrich syndrome protein gene and their effects on transcriptional, translational, and clinical phenotypes. *Hum. Mutat.* [published online ahead of print: 1999]; doi:10.1002/(SICI)1098-1004(1999)14:1<54::AID-HUMU7>3.0.CO;2-E

6. Orange JS, Stone KD, Turvey SE, Krzewski K. The Wiskott-Aldrich syndrome. *Cell. Mol. Life Sci.* 2004; doi:10.1007/s00018-004-4086-z

7. Comrie WA et al. Genetic immunodeficiency and autoimmune disease reveal distinct roles of *Hem1* in the WAVE2 and mTORC2 complexes. *bioRxiv* [published online ahead of print: 2019]; doi:10.1101/692004

8. Peters LA et al. A functional genomics predictive network model identifies regulators of inflammatory bowel disease. *Nat. Genet.* [published online ahead of print: 2017]; doi:10.1038/ng.3947

9. Dickinson JD et al. Genomic abnormalities in chronic lymphocytic leukemia influence gene expression by a gene dosage effect. *Int. J. Mol. Med.* [published online ahead of print: 2006]; doi:10.3892/ijmm.17.5.769

10. Kunda P, Craig G, Dominguez V, Baum B. Abi, Sra1, and Kette Control the Stability and Localization of SCAR/WAVE to Regulate the Formation of Actin-Based Protrusions. *Curr. Biol.* [published online ahead of print: 2003]; doi:10.1016/j.cub.2003.10.005

11. Soto MC et al. The GEX-2 and GEX-3 proteins are required for tissue morphogenesis and cell migranons in C. elegans. *Genes Dev.* [published online ahead of print: 2002]; doi:10.1101/gad.955702

12. Djakovic S, Dyachok J, Burke M, Frank MJ, Smith LG. BRICK 1/HSPC300 functions with SCAR and the ARP2/3 complex to regulate epidermal cell shape in Arabodopsis. *Development* [published online ahead of print: 2006]; doi:10.1242/dev.02280

13. Ibarra N, Blagg SL, Vazquez F, Insall RH. Nap1 Regulates Dictyostelium Cell Motility and Adhesion through SCAR-Dependent and -Independent Pathways. *Curr. Biol.* [published online ahead of print: 2006]; doi:10.1016/j.cub.2006.02.068

14. Weiner OD et al. Hem-1 complexes are essential for Rac activation, actin polymerization, and myosin regulation during neutrophil chemotaxis. *PLoS Biol.* 2006;4(2):186–199.

15. Park H et al. A point mutation in the murine *Hem1* gene reveals an essential role for Hematopoietic Protein 1 in lymphopoiesis and innate immunity [Internet]. *J.*

Exp. Med. 2008;205(12):2899 LP – 2913.

16. Shi J, Hua L, Harmer D, Li P, Ren G. Cre driver mice targeting macrophages. In: *Methods in Molecular Biology*. 2018:

17. Madisen L et al. A robust and high-throughput Cre reporting and characterization system for the whole mouse brain. *Nat. Neurosci.* [published online ahead of print: 2010]; doi:10.1038/nn.2467

18. Park H et al. A point mutation in the murine Heml gene reveals an essential role for Hematopoietic Protein 1 in lymphopoiesis and innate immunity. *J. Exp. Med.* 2008;205(12). doi:10.1084/jem.20080340

19. Shao L et al. The Wave2 scaffold Hem-1 is required for transition of fetal liver hematopoiesis to bone marrow. *Nat. Commun.* [published online ahead of print: 2018]; doi:10.1038/s41467-018-04716-5

20. Todd EM et al. Alveolar macrophage development in mice requires L-plastin for cellular localization in alveoli. *Blood* [published online ahead of print: 2016]; doi:10.1182/blood-2016-03-705962

21. Schneider C et al. Alveolar Macrophages Are Essential for Protection from Respiratory Failure and Associated Morbidity following Influenza Virus Infection. *PLoS Pathog.* [published online ahead of print: 2014]; doi:10.1371/journal.ppat.1004053

22. Li J, Lee DSW, Madrenas J. Evolving Bacterial Envelopes and Plasticity of TLR2-Dependent Responses: Basic Research and Translational Opportunities. *Front. Immunol.* [published online ahead of print: 2013]; doi:10.3389/fimmu.2013.00347

23. Kopf M, Schneider C, Nobs SP. The development and function of lung-resident macrophages and dendritic cells. *Nat. Immunol.* 2015; doi:10.1038/ni.3052

24. Purnama C et al. Transient ablation of alveolar macrophages leads to massive pathology of influenza infection without affecting cellular adaptive immunity. *Eur. J. Immunol.* [published online ahead of print: 2014]; doi:10.1002/eji.201344359

25. Tate MD, Pickett DL, van Rooijen N, Brooks AG, Reading PC. Critical Role of Airway Macrophages in Modulating Disease Severity during Influenza Virus Infection of Mice. *J. Virol.* [published online ahead of print: 2010]; doi:10.1128/jvi.00291-10

26. Kumagai Y et al. Alveolar Macrophages Are the Primary Interferon-α Producer in Pulmonary Infection with RNA Viruses. *Immunity* [published online ahead of print: 2007]; doi:10.1016/j.immuni.2007.07.013

27. Yu X et al. The Cytokine TGF-β Promotes the Development and Homeostasis of Alveolar Macrophages. *Immunity* [published online ahead of print: 2017]; doi:10.1016/j.immuni.2017.10.007

28. Seo SU et al. Type I interferon signaling regulates Ly6Chi monocytes and neutrophils during acute viral pneumonia in mice. *PLoS Pathog.* [published online ahead of print: 2011]; doi:10.1371/journal.ppat.1001304

29. Deady LE et al. L-plastin is essential for alveolar macrophage production and control of pulmonary pneumococcal infection. *Infect. Immun.* [published online ahead of print: 2014];

doi:10.1128/IAI.01199-13

30. Schneider C et al. Induction of the nuclear receptor PPAR-γ 3 by the cytokine GM-CSF is critical for the differentiation of fetal monocytes into alveolar macrophages. *Nat. Immunol.* [published online ahead of print: 2014]; doi:10.1038/ni.3005

31. Trapnell BC, Whitsett JA. GM-CSF Regulates Pulmonary Surfactant Homeostasis and Alveolar Macrophage-Mediated Innate Host Defense. *Annu. Rev. Physiol.* [published online ahead of print: 2002]; doi:10.1146/annurev.physiol.64.090601.113847

32. Nakamura A et al. Transcription repressor Bach2 is required for pulmonary surfactant homeostasis and alveolar macrophage function. *J. Exp. Med.* [published online ahead of print: 2013]; doi:10.1084/jem.20130028

33. Bonfield TL et al. Peroxisome Proliferator-Activated Receptor-γ Is Deficient in Alveolar Macrophages from Patients with Alveolar Proteinosis. *Am. J. Respir. Cell Mol. Biol.* [published online ahead of print: 2003]; doi:10.1165/rcmb.2003-0148OC

34. Suzuki T et al. Pulmonary macrophage transplantation therapy. *Nature* [published online ahead of print: 2014]; doi:10.1038/nature13807

35. Stark MA et al. Phagocytosis of apoptotic neutrophils regulates granulopoiesis via IL-23 and IL-17. *Immunity* [published online ahead of print: 2005]; doi:10.1016/j.immuni.2005.01.011

36. Friedel RH, Wurst W, Wefers B, Kühn R. Generating Conditional Knockout Mice. In: 2010:

37. Clausen BE, Burkhardt C, Reith W, Renkawitz R, Förster I. Conditional gene targeting in macrophages and granulocytes using LysMcre mice. *Transgenic Res.* [published online ahead of print: 1999]; doi:10.1023/A:1008942828960

38. Habib T et al. Myc stimulates B lymphocyte differentiation and amplifies calcium signaling. *J. Cell Biol.* [published online ahead of print: 2007]; doi:10.1083/jcb.200704173

39. Evrard M et al. Developmental Analysis of Bone Marrow Neutrophils Reveals Populations Specialized in Expansion, Trafficking, and Effector Functions.. *Immunity* 2018;48(2):364-379.e8.

40. Ginhoux F. Fate PPAR-titioning: PPAR-γ 3 “instructs” alveolar macrophage development. *Nat. Immunol.* [published online ahead of print: 2014]; doi:10.1038/ni.3011

41. Bradford MM. A rapid and sensitive method for the quantitation of microgram quantities of protein utilizing the principle of protein-dye binding. *Anal. Biochem.* [published online ahead of print: 1976]; doi:10.1016/0003-2697(76)90527-3

42. Zengel P et al. μ-Slide Chemotaxis: A new chamber for long-term chemotaxis studies. *BMC Cell Biol.* [published online ahead of print: 2011]; doi:10.1186/1471-2121-12-21

43. Bzymek R et al. Real-time two- and three-dimensional imaging of monocyte motility and navigation on planar surfaces and in collagen matrices: Roles of Rho. *Sci. Rep.* [published online ahead of print: 2016]; doi:10.1038/srep25016

44. Rittirsch D et al. Acute Lung Injury Induced by Lipopolysaccharide Is Independent of Complement Activation. *J. Immunol.* [published online ahead of print: 2014]; doi:10.4049/jimmunol.180.11.7664

45. Knapp S et al. Pulmonary Lipopolysaccharide (LPS)-Binding Protein Inhibits the LPS-

Induced Lung Inflammation In Vivo[published online ahead of print: 2018]; doi:10.4049/jimmunol.176.5.3189

46. Nayak DK, Mendez O, Bowen S, Mohanakumar T. Isolation and In Vitro Culture of Murine and Human Alveolar Macrophages2018;(April):1–8.

47. Hu Y, Hu X, Boumsell L, Ivashkiv LB. IFN-γ and STAT1 Arrest Monocyte Migration and Modulate RAC/CDC42 Pathways. *J. Immunol.* [published online ahead of print: 2008]; doi:10.4049/jimmunol.180.12.8057

48. Weischenfeldt J, Porse B. Bone marrow-derived macrophages (BMM): Isolation and applications. *Cold Spring Harb. Protoc.* [published online ahead of print: 2008]; doi:10.1101/pdb.prot5080

49. Linehan E et al. Aging impairs peritoneal but not bone marrow-derived macrophage phagocytosis. *Aging Cell* [published online ahead of print: 2014]; doi:10.1111/acel.12223

50. Kamei A et al. Exogenous remodeling of lung resident macrophages protects against infectious consequences of bone marrow-suppressive chemotherapy. *Proc. Natl. Acad. Sci. U. S. A.* [published online ahead of print: 2016]; doi:10.1073/pnas.1607787113

51. Croons V, Martinet W, Herman AG, Timmermans JP, De Meyer GRY. Selective clearance of macrophages in atherosclerotic plaques by the protein synthesis inhibitor cycloheximide. *J. Pharmacol. Exp. Ther.* [published online ahead of print: 2007]; doi:10.1124/jpet.106.113944

52. Tan Y, Zanoni I, Cullen TW, Goodman AL, Kagan JC. Mechanisms of Toll-like Receptor 4 Endocytosis Reveal a Common Immune-Evasion Strategy Used by Pathogenic and Commensal Bacteria. *Immunity* [published online ahead of print: 2015]; doi:10.1016/j.immuni.2015.10.008

53. Wolf AI et al. Protective antiviral antibody responses in a mouse model of influenza virus infection require TACI. *J. Clin. Invest.* [published online ahead of print: 2011]; doi:10.1172/JCI57362

54. Stark A-K, Stark A-K, Banham-Hall E, Okkenhaug K. Acute Streptococcus pneumoniae lung infection: Mouse model and characterisation of the immune response. [Internet]. *Protoc. Exch.* [published online ahead of print: September 24, 2018]; doi:10.1038/protex.2018.114